Archaeological and Anthropological Sciences (2023) 15:15
https://doi.org/10.1007/s12520-022-01710-3

RESEARCH

The technology of ancient lime mortars from the Żejtun Roman Villa (Malta)

R. Fort[1] · M. J. Varas-Muriel[1,2] · D. Ergenç[1,3] · J. Cassar[4] · M. Anastasi[5] · N. C. Vella[5]

Received: 26 July 2022 / Accepted: 19 December 2022 / Published online: 13 January 2023
© The Author(s) 2023

Abstract

Studies on original mortars can greatly assist archaeological interpretations, as elucidating the composition of such mortars gives clues on the origin of raw materials, manufacturing technology, and the construction phases of a site. This article presents the multi-analytical characterisation of 24 mortars and plasters from the Żejtun Roman Villa, Malta, to support archaeological hypotheses on the history of the construction of the site. The samples, belonging to at least three distinct phases included in the stratigraphy of the Żejtun archaeological site, were analysed using polarised light microscopy (PLM), scanning electron microscopy (SEM–EDS), X-ray diffraction (XRD), thermogravimetry (TGA/DSC), X-ray fluorescence (XRF), ion chromatography (IC), and stable isotope analysis (^{13}C and ^{18}O). The assessment of the results through correlations with archaeological evidence identifies five types of mortars with varying degrees of hydraulicity. These are associated with different development phases of the site and distinctive uses and were mainly produced using local resources, except in the Early Roman period when natural pozzolanic raw materials started being used. As there are no natural pozzolans on the Maltese Islands, it is hypothesised that the pozzolanic materials used as aggregate in the mortars were imported to the Islands from neighbouring volcanic regions. This volcanic aggregate was especially abundant in one of the mortar types, which was used mainly as a bedding mortar for floors.

Keywords Mortars · Plasters · Raw materials · Provenance · Petrography · Isotopes

Introduction

Roman technology for making lime mortars and plasters spread throughout the Mediterranean. Thanks at least in part to their quality and durability, many Roman monuments and cities have survived to this day (Degryse et al. 2002; Riccardi et al. 2007; Yaseen et al. 2013; Drdácký et al. 2013; Cardoso et al. 2014; Columbu et al. 2018; Vitti 2021). The mixing of aerial lime and a reactive aggregate such as volcanic ash (*pozzolana*), which created a material with hydraulic properties, was a great technological achievement attributable to the Romans (DeLaine 2021; Lancaster 2021). The availability of resources to produce hydraulic mortars was however not uniform, although *pozzolana* was widely exported from its source locations, other regions had to adapt mortar recipes to locally available materials. Artificial pozzolanic materials, such as crushed ceramics (*cocciopesto/opus signinum*), were also utilised for their hydraulic qualities as well as their wide availability (Yaseen et al. 2013; Fichera et al. 2015; Miriello et al. 2015; Columbu and Garau 2017; Ergenç and Fort 2019; Columbu et al. 2019; Lancaster 2021; Vitti 2021; Seymour et al. 2022). The binder commonly used by the Romans was aerial lime, obtained from burning pure limestone, systematically rejecting clayey limestone (Rassineux et al. 1989; Lancaster 2021).

In the Maltese archipelago, no detailed scientific studies have ever been carried out to characterise archaeological

✉ R. Fort
rafael.fort@csic.es

1 Instituto de Geociencias (CSIC, UCM) C/Doctor Severo Ochoa 7, Madrid, Spain

2 Facultad Ciencias Geológicas, Universidad Complutense de Madrid (UCM), C/José Antonio Novais 12, 28040 Madrid, Spain

3 Conservation of Cultural Heritage Graduate Program, Department of Architecture, Middle East Technical University, 06800 Ankara, Turkey

4 Department of Conservation and Built Heritage, Faculty for the Built Environment, University of Malta, Msida MSD 2080, Malta

5 Department of Classics and Archaeology, Archaeology Centre, University of Malta, Msida 2080, MSD, Malta

mortars and assess their composition, function, or the source of any potentially imported pozzolanic aggregate. The site of a rural structure in Żejtun (35° 51′ 06.3″ N, 14° 32′ 08.6″ E) in the southern region of the Island of Malta (Fig. 1) is one of a few Roman Villa complexes on the island that has survived the effects of heavy urban sprawl and industrial development over the last century (Anastasi and Vella 2018). The villa is not monumental in the way many other Roman sites are; construction and modification of structures over several centuries, coupled with the effects of spoliation, destruction, and agriculture in more recent times, have resulted in a transformation in which fragments or material residues are arguably the most significant remains.

Through extensive archaeological excavations, the remains of the Żejtun Villa site have revealed a complex structure characterised by a series of construction and rebuilding activities straddling the Punic and Roman periods (Vella et al. 2018). The different construction techniques employed at the site, combined with the careful stratigraphic approach followed in the recent excavations, make it a suitable site for studying ancient building mortars and plasters, a first time such a comprehensive study has been carried out in the Maltese Islands.

The purpose of this study was to establish the type and source of the geomaterials utilised and also to try to determine whether a link exists between the composition of the mortar, its specific use, and the construction technique/s used on site, as well as whether any chronological differences could be detected in the mortars used. Another important aspect was to recognise any technological variations in the mortar mixes that could subsequently allow archaeologists to classify other local mortars found in the archaeological record, with associations linked to their function, source, and period. Such information would serve to produce a database of archaeological and historical mortars and plasters and also inform any conservation interventions needed at this particular site and in similar sites in the Maltese Islands.

The historical context of Żejtun Villa site

The site's cultural history is complex. It was first discovered in 1961 during construction works and was explored further in 1964, and full-scale archaeological excavations were carried out between 1972 and 1976 (Bonanno and Vella 2012). These campaigns did not adopt a stratigraphic approach, and a final report collating the results has never been found. The site languished in a state of near abandonment for three decades until renewed work began in 2006 by the University of Malta.

The 1970s excavations had revealed extensive structural features constructed using a combination of large *Globigerina* Limestone ashlar blocks and irregular rubble building techniques, immediately thought to belong to a Roman Villa of the rustic type, combining a residential and an industrial area (Bonanno 2018). A series of floors paved with ceramic tiles was also discovered, partitioned by the base foundations of walls built in irregular rubble stones and rendered with decorated wall plaster. To the north of these rooms lay an area retaining stone vats and a counterweight stone associated with the pressing of olives to make oil (Bonanno and Vella 2012; Anastasi and Vella 2018; Anastasi et al. 2022) . A double-entrance cistern partly hewn in the rock and partly constructed out of ashlar masonry was also discovered to the south of the site (Fig. 2).

The renewed excavations between 2006 and 2018 were concentrated on exploring previously unexcavated areas to the south and east of the main structure (Bonanno and Vella 2012; Vella et al. 2017). These campaigns showed that the entire complex was constructed directly upon the bedrock. However, because the ground is uneven and slopes by a gradient of about 1.5 m from north to south, foundations were raised at the south and southeast to the level of the structures to the north and west (Fig. 3). These foundations consist of orthogonal walls, up to three courses high, built to provide a sturdy base for overlying structures (now missing) and to lay floors. Most of the archaeological deposits, which have been investigated in these renewed excavations, belong to the fills that were deposited within the spaces defined by these foundation walls.

The construction and occupation of the site can be divided into at least three broad phases. Additional phases have been recognised based on diverse building activities as well as evidence of structural modifications or abandonment and destruction (Table 1). The pre-villa phase (phase 1) is associated with a vineyard, a 'double-entrance' cistern, and remains of a built structure of unknown function, which have been dated on the basis of pottery style to the Late Punic/Early Roman period (c. fourth to second centuries BCE) (Vella et al. 2018). The vineyard and structure were abandoned and covered over by the construction of a villa complex with an area reserved for the pressing of olives to make oil (phase 2). Most of the surviving masonry, floors, and structures at the site are associated with this phase, where pottery has provided a terminus post quem of the end of the second/first century BCE for the abandonment of the vineyard and the construction of the villa. Parts of the residential area have been defined, including the foundations of what would have been a peristyle. Prolonged occupation, maintenance of the villa complex, and a reconfiguration of the olive pressing room are evidenced by the accumulation of debris from earlier structures and features mixed within levelling fills associated with building extensions in the north-east of the site and re-plastered walls in the residential area. These activities took place over a span of time stretching from the early Imperial period (late first century BCE/first century) to the Late

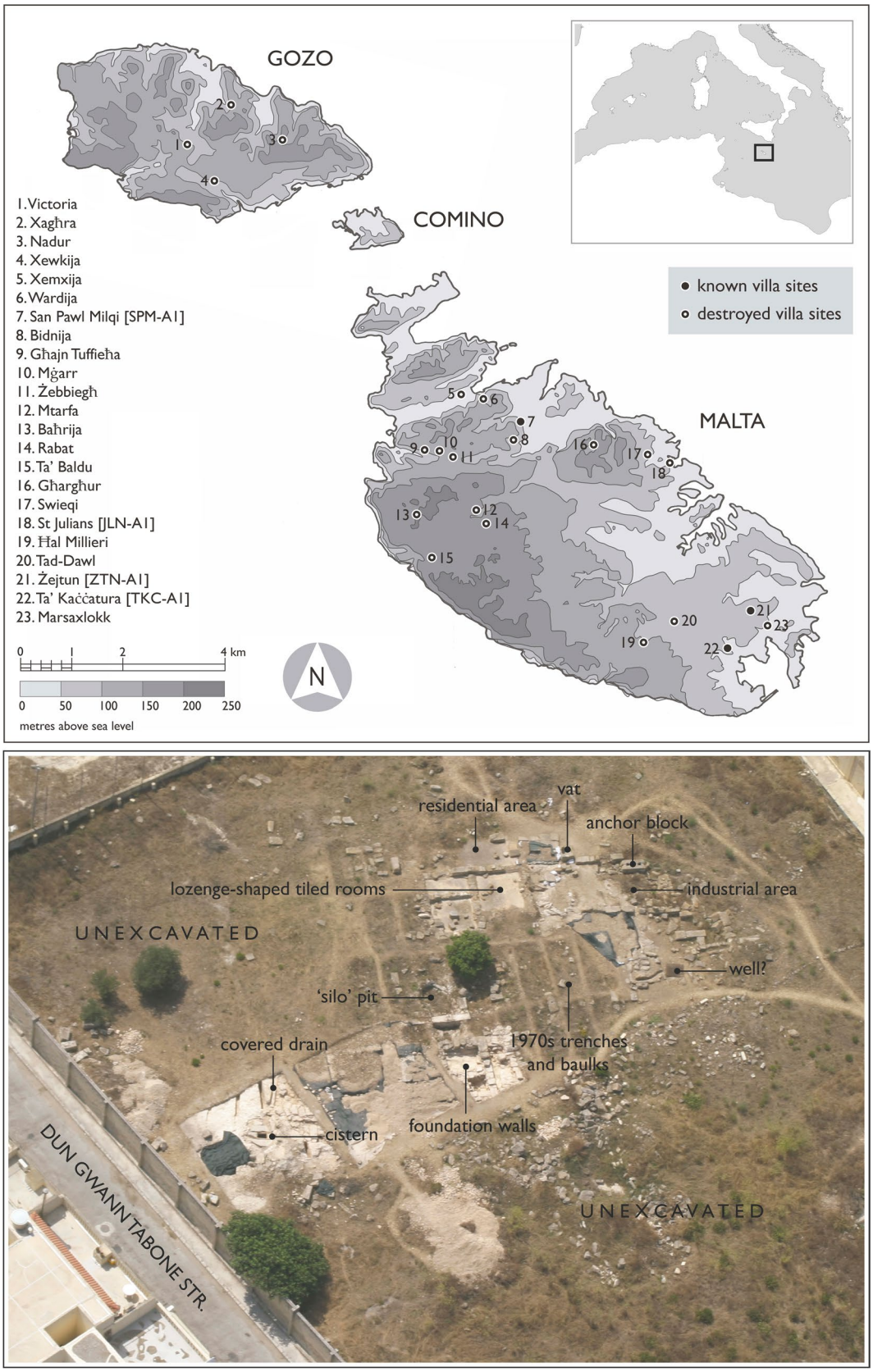

Fig. 1 Location map of the archaeological site of Żejtun Roman Villa (Malta) (35° 51′ 06.3″ N, 14° 32′ 08.6″ E)

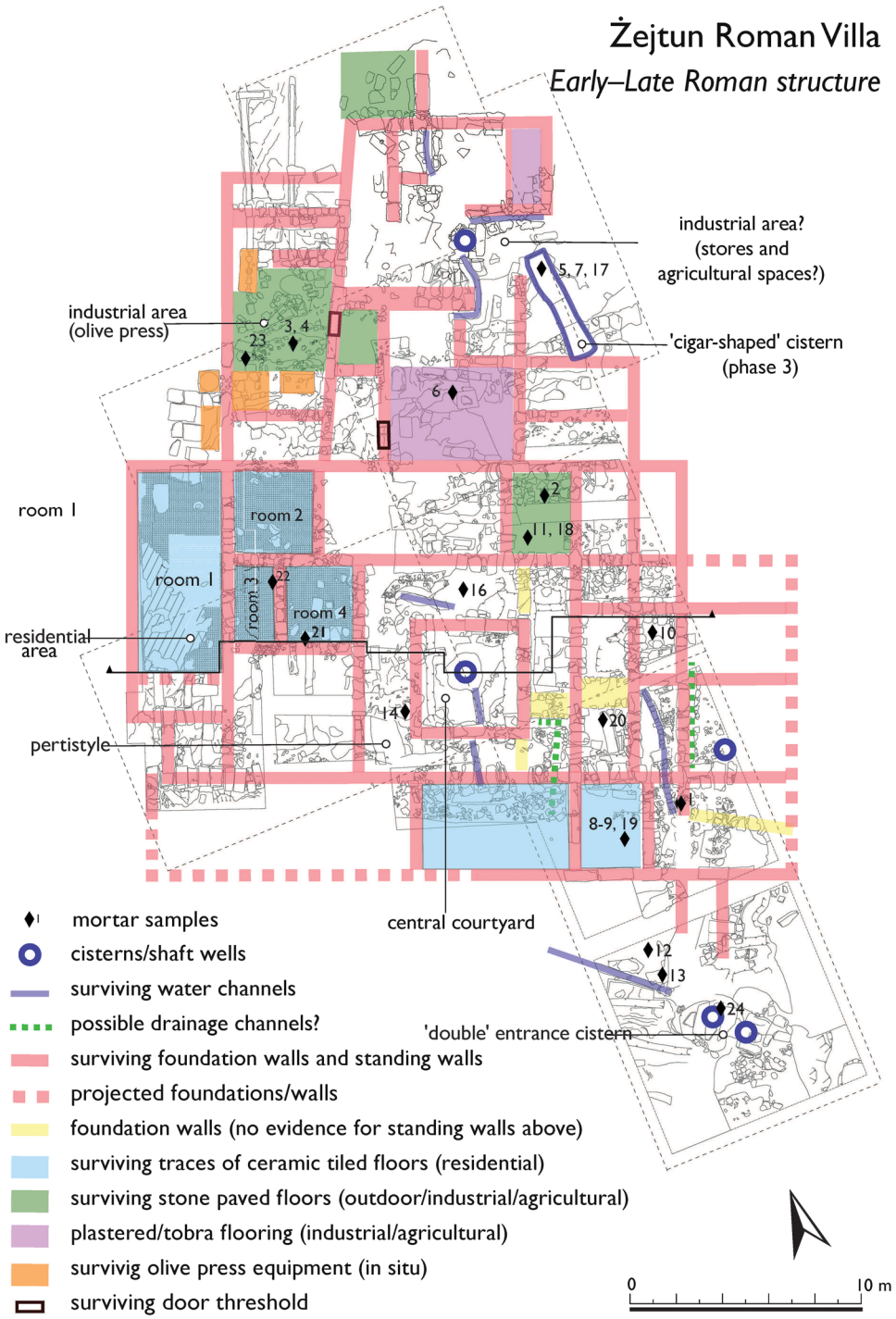

Fig. 2 Reconstructed floor plan of the archaeological site

Roman period (late Third/fourth century CE) based on the pottery and coins found (Anastasi 2012; Vella et al. 2018).

The villa appears to have been abandoned and fell into ruin sometime after the fifth century CE, based on the accumulation of abandonment deposits with pottery dating to the fifth to seventh century CE and eighth to tenth century CE. This post−villa phase (phase 3) is also associated with extensive spoliation activity marked by the removal of much of the then visible structure and foundation walls, presumably for reuse elsewhere. At some point following the abandonment of the villa, a large 'cigar-shaped' cistern was cut into the rock, directly through earlier structures; this has been linked to Byzantine or Early Medieval use of the site for agricultural purposes. This cistern eventually collapsed as a result of the

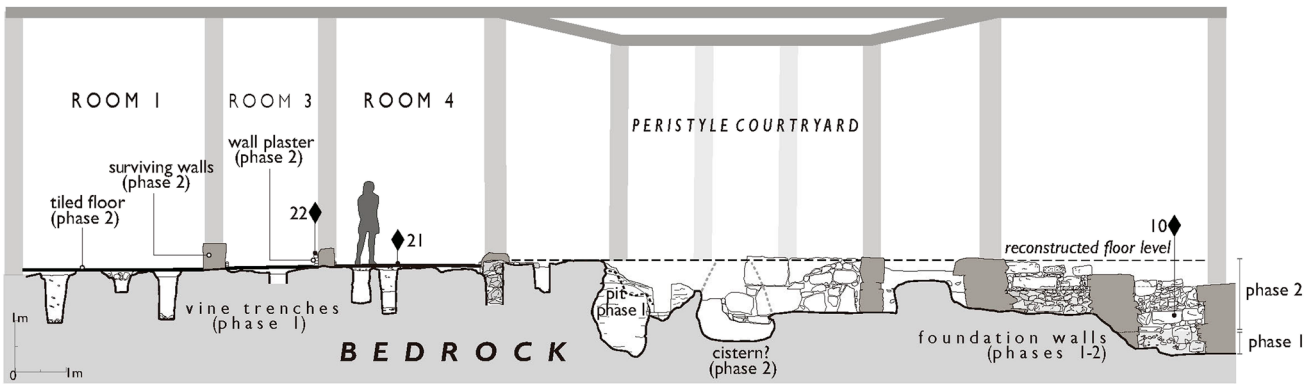

Fig. 3 West–east section marked in Fig. 2 of the archaeological site

Table 1 Table listing the main construction phases at the Żejtun villa site and the location of the samples analysed

Phase	Date	Construction activities	Sample name
1. Pre-villa	c. fourth to secnd c. BCE	Vineyard, pre-villa structure and 'double-entrance' cistern	MA-24
2. Villa	c. second/first c. BCE–third/fourth c. CE	Construction of main villa complex (over abandoned vineyard) with olive press and residential area; occupation, maintenance and re-building of villa	MA-1, MA-2, MA-3, MA-4, MA-6, MA-8, MA-9, MA-10, MA-12, MA-13, MA-14, MA-19, MA-20, MA-21, MA-22, MA-23
3. Post-villa	Fifth to seventh c. CE to recent	Abandonment and spoliation of Villa complex; use of site for agricultural purpose	MA-5, MA-7, MA-11, MA-15, MA-16, MA-17, MA-18

poor nature of the bedrock and naturally occurring fissures in the rock and was abandoned shortly after. Rubble filled the abandoned cavity from the mid-eighteenth century, based on the latest–dated pottery identified within its fill.

The geological setting of site

The villa is located within the grounds of a school on the outskirts of the Żejtun village (Fig. 1). It is built directly upon a limestone bedrock belonging to the miocenic (Aquitaian) Lower Globigerina Limestone Formation (Scerri 2019), consisting of marine bioclastic limestones (medium to fine-grained wackestone-packstone) yellowish to greyish in colour. It is dominated by planktonic micro-foraminifera (Baldassini and Di Stefano 2017), primarily globigerinae. The geological formation is massive, poorly to moderately consolidated, and intensely burrowed (Pedley 1976).

The three geological members forming the Globigerina Limestone Formation (Lower, Middle, and Upper Globigerina Limestone) are separated by hard and rubefacted[1] surfaces (hardgrounds) rich in phosphates. These beds, due to erosion, include conglomerates with dark brown rubefacted edges, a phosphatized crust, and clay accumulations containing glauconite (Pedley 1976; Pedley and Bennett 1985; Rose et al. 1992; Gruszczynski et al. 2008; Bianucci et al. 2011; Foresi et al. 2014; Chatzimpaloglou et al. 2020).

Materials and methods

Sampling

A total of 24 mortars and plasters were sampled, including wall joint mortars and plasters, tile-laying bedding mortars, and cistern linings and shuttering layers. The sampling took place in two stages. The first 20 samples were selected from a broad range of archaeological deposits that had been excavated between 2006 and 2014. Many of these deposits were formed in the post-villa phase (phase 3), but were found to consist of residual mortar fragments that are associated with the construction, maintenance, and abandonment of the main villa complex (phase 2). Many of these initial samples consist of residual fragments that were selected from archaeological deposits that were excavated by hand and identification based on the sample's perceived function (Table 2). Similar mortars could not be traced on any of the surviving standing structures, suggesting that these samples belong to the constructions that were

[1] The process of red colouring is the result of the formation of hematite.

abandoned and destroyed previously. They were also selected based on the ability of the archaeologists to securely date the stratigraphic contexts these samples were located in. Six samples were composed of multiple layers, each of which was in this study divided into sub-samples and analysed separately.[2]

A second stage of sampling took place, following the promising analytical results of the first batch of samples. It was decided that an additional four samples would be selected from existing mortars that had survived in situ. Table 2 lists the samples collected and summarises the associated chronological, contextual, typological, and functional evidence obtained through the archaeological record and analyses of materials.

Analytical techniques

A variety of complementary techniques are now commonly used to characterise mortars (Ergenç et al. 2021) and hence to help reconstruct the source and function of these specific building components in an archaeological context.

In this case, a petrographic study was first conducted using thin sections, which were partially stained with alizarin to highlight the calcite-containing areas (Dickson 1966). The thin sections were viewed under a JENAPOL polarised light optical microscope (PLM) fitted with a Canon 650 digital camera to determine the composition, texture, and microstructure of the different samples (Elsen 2006). The same thin sections were also polished and coated with graphite and examined using a scanning electron microscope (SEM) with backscattered electron detection mode (BSE) and microanalysis using energy dispersive X-rays (EDS) to investigate the microstructure and chemical composition of the binders and aggregates. The instrument used was a JEOL JSM 6400 SEM, with a voltage range of 0.2 to 40 kV and a vacuum of 10−5 Torr; the microanalyzer was an Oxford Inca EDS.

X-ray diffraction (XRD) of powdered (< 53 μm) samples (enriched binder) was used for mineralogical characterisation. This technique supports and confirms the composition described by PLM. The equipment used was a PHILIPS PW 1752 diffractometer, and the conditions used were 40 kV and 30 mA with a Cu anode and graphite monochromator. The diffractograms were obtained at a range between 2 and 65°, and at a speed of 2° per minute.

TGA/DSC analysis was performed using a TA Instrument SDT-Q600 and simultaneously a thermogravimetric analyser General V4.1C 200 DuPont under N2, with a heating rate of 10 °C per minute. The analysis was performed on ground samples of the binder only, previously mechanically separated from the large aggregates of the mortars. TGA/DSC analysis of the samples gave the percentages of weight losses, working with the following temperature ranges: up to 120 °C, between 120 and 200 °C, between 200 and 600 °C, and above 600 °C. All ensuing reactions are endothermic and are due to weight losses attributable to the dehydration (< 120 °C), dehydration of hydrated salts (120–200 °C), dehydration of hydraulic compounds (200–600 °C), and decomposition-decarboxylation (> 600 °C) of the Ca-carbonate (from the lime binder) and other existing minerals within these mortars. Weight losses between 200 and 600 °C (bound H2O in hydraulic compounds or CO2 deriving from the reactions between Ca-carbonate and silicates according to the following reaction: $CaCO3 + XSiO2 \Rightarrow CaXSiO3 + CO2$ (where X = K, Al, F) (400–600 °C) (Columbu et al. 2017 and Columbu and Garau 2017) and > 600 °C (CO2 release after carbonate decomposition) were used to interpret the hydraulic degree of the mortars (Bakolas et al. 1995; Biscontin et al. 2002; Maravelaki-Lalaitzaki et al. 2003; Moropoulou et al. 2000; 2005; Genestar et al. 2006; Lawrence 2006; Ergenç et al. 2021).

The chemical composition of the mortars was defined using a portable XRF instrument (THERMO NITON XL3t GOLDD rays) with X-rays generated between 50 kV and 100 μÅ. Three zones of each sample were measured, each comprising 8 mm of fresh surface, with an analysis time of 65 s.

In the 24 studied samples from the archaeological site, the isotope ratios of 18O and 13C were determined using a MAT-252 spectrometer coupled with a Thermo Scientific™ KIEL DEVICE III from Thermofisher. RC-1 standards were used (δ 13C = 2.83 and δ 18O = −2.08) as well as CECC standards (δ 13C = −20.77 ± 0.03 ‰ and δ 18O = −17.56 ± 0.06. All results are shown with respect to the international reference standard Vienna belemnite Pee Dee (VPDB) (Craig 1957).

Results

The analysed samples can be divided into five distinct groups (T1–T5) based on the characteristics of the aggregate and binder used (Table 2).

Petrographic and mineralogical characterisation (PLM, XRD, SEM–EDS)

Type 1: mortar with limestone fragments (samples MA-1, MA-2C, MA-3, MA-8, MA-9, MA-19B, MA-22B, MA-24B).

This mortar type shows beige to ochre tones and is characterised by a homogenous and cohesive binder (Fig. 4a). Aggregates comprise 60–75% of the sample,with poorly sorted coarse grains up to 6 mm in size. The aggregate:binder ratio is estimated at 3:2 to 3:1. This angular aggregate is composed of

[2] These sub-samples were labelled with the following letters: (A) outer layer, (B) intermediate layer, and (C) inner layer (closest to substrate).

Table 2 Table listing the samples, their actual location of recovery (whether residual or in situ), the mortar type and proposed origin, and function on site based on the results of the analyses. The five types of mortars differentiated petrographically (T1 to T5), and the degree of hydraulicity are incorporated (*H*, Hydraulic; *HH*, High hydraulic; *NH*, Non-hydraulic)

Sample no	Context phase	Actual location	Petrological types					Hydraulicity	Proposed location	Proposed function
			T1	T2	T3	T4	T5			
MA-1	Phase 2	Re-used in villa	•					HH	Pre-Villa structure	Vat lining
MA-2	Phase 2	Residual in levelling fill	2C	2B	2A			H[C], NH[B,A]	Villa	Painted wall render
MA-3	Phase 2	Residual in spoliation fill	•					NH	Villa	Joint mortar for masonry
MA-4	Phase 2	Residual in spoliation fill		•				NH	Villa	Render/joint mortar
MA-5	Phase 3	Residual					•	HH	Villa	Bedding mortar for tiled floor
MA-6	Phase 3	Residual		•				NH	Villa	Wall render
MA-7	Phase 3	Residual					•	HH	Villa	Shuttering render
MA-8	Phase 2	Residual in levelling fill	•					H	Pre-villa structure	Painted wall render
MA-9	Phase 2	Residual in levelling fill	•					NH	Pre-villa structure	Wall render
MA-10	Phase 2	Residual in foundation fill				•		H	Villa	*Cocciopesto* floor/lining
MA-11	Phase 3	Residual				•		H	Villa	*Cocciopesto* floor/lining
MA-12	Phase 2	Residual					•	NH	Villa	Wall render/bedding mortar?
MA-13	Phase 2	Residual					•	HH	Villa	Wall render
MA-14	Phase 2	Residual					•	HH	Villa	Bedding mortar for tiled floor
MA-15	Phase 3	Residual					•	HH	Villa	Bedding mortar for tiled floor
MA-16	Phase 3	Residual					•	HH	Villa	Bedding mortar for tiled floor
MA-17	Phase 3	Residual				17B	17A	H[A], HH[B]	Villa	Wall render
MA-18	Phase 3	Residual		18B	18A			H[B], NH[A]	Villa	Wall render
MA-19	Phase 2	Residual in levelling fill	19B	19C	19A			NH[C-A]	Pre-villa structure	Painted wall render
MA-20	Phase 2	In situ (?) in re-used press element (?)		•				NH	Pre-villa structure	Joint mortar for masonry
MA-21	Phase 2	In situ tiled floor					•	HH	Villa	Bedding mortar for tiled floor
MA-22	Phase 2	In situ wall render	22B		22A			NH[A]	Villa	Painted wall render
MA-23	Phase 2	In situ lining		•				NH	Villa	Vat lining
MA-24	Phase 1	In situ cistern	24B		24A			HH[B]	Pre-villa/villa	Cistern lining

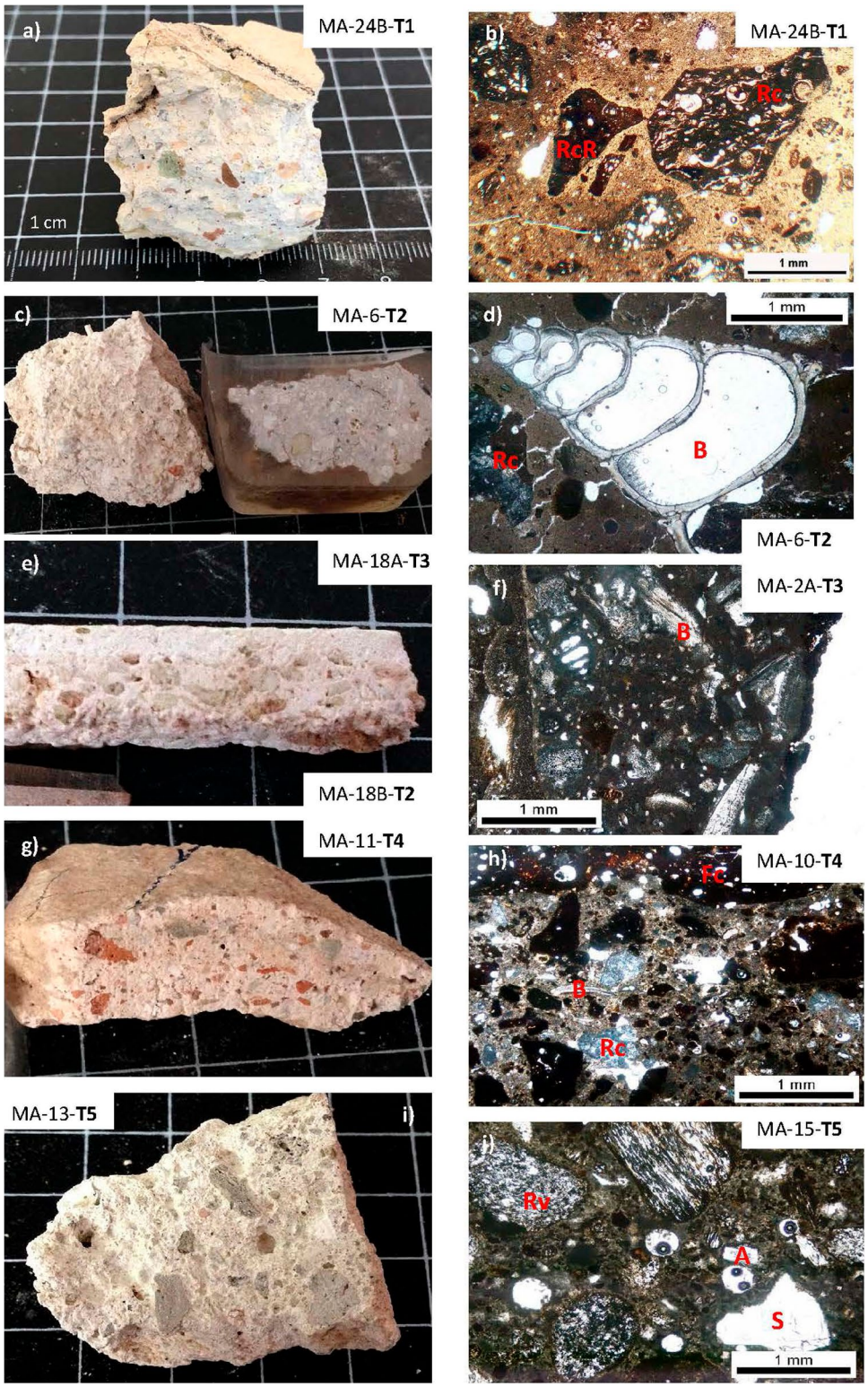

Fig. 4 Visual aspect (left photo, a, c, e, g, i) and under petrographic microscope in parallel polarised light mode (right photo, b, d, f, h, j) of five identified types of mortars (T1 to T5). **a**, **b** Mortars with marl/limestone fragments and rubefacted grains. **c**, **d** Mortars with marl/limestone fragments and bioclasts. **e**, **f** Mortars with bioclasts. **g**, **h** Mortars with ceramic fragments, marl/limestone fragments, and bioclasts. **i**, **j** Mortars with volcanic rock fragments and isolated sanidine crystals. Rc, limestone and marl fragments; RcR, rubefacted marl fragments; B, bioclast fragments; Fc, ceramic fragments; Rv, volcanic rock fragments; S, sanidine; A, augite

limestone (> 90% CaO) and clayey marl (> 30% CaO, > 65% SiO_2-Al_2O_3-K_2O) fragments containing planktonic microforaminifera (globigerinae and biserial packstone) (Dunham 1962) (Figs. 4b, 5a, and 6a). Many of these marl fragments appear rubefacted (hardground grains) (> 5% FeO and 15–32% CaO) (Fig. 5a, b). In some of the plaster samples of Type 1 (MA-1, MA-2C, MA-3), ceramic fragments (5–10%) measuring < 1 mm in size are present, together with some black particles (ash). The ceramic fragments belong to two types (Fig. 6b). The first type is characterised as very porous, with

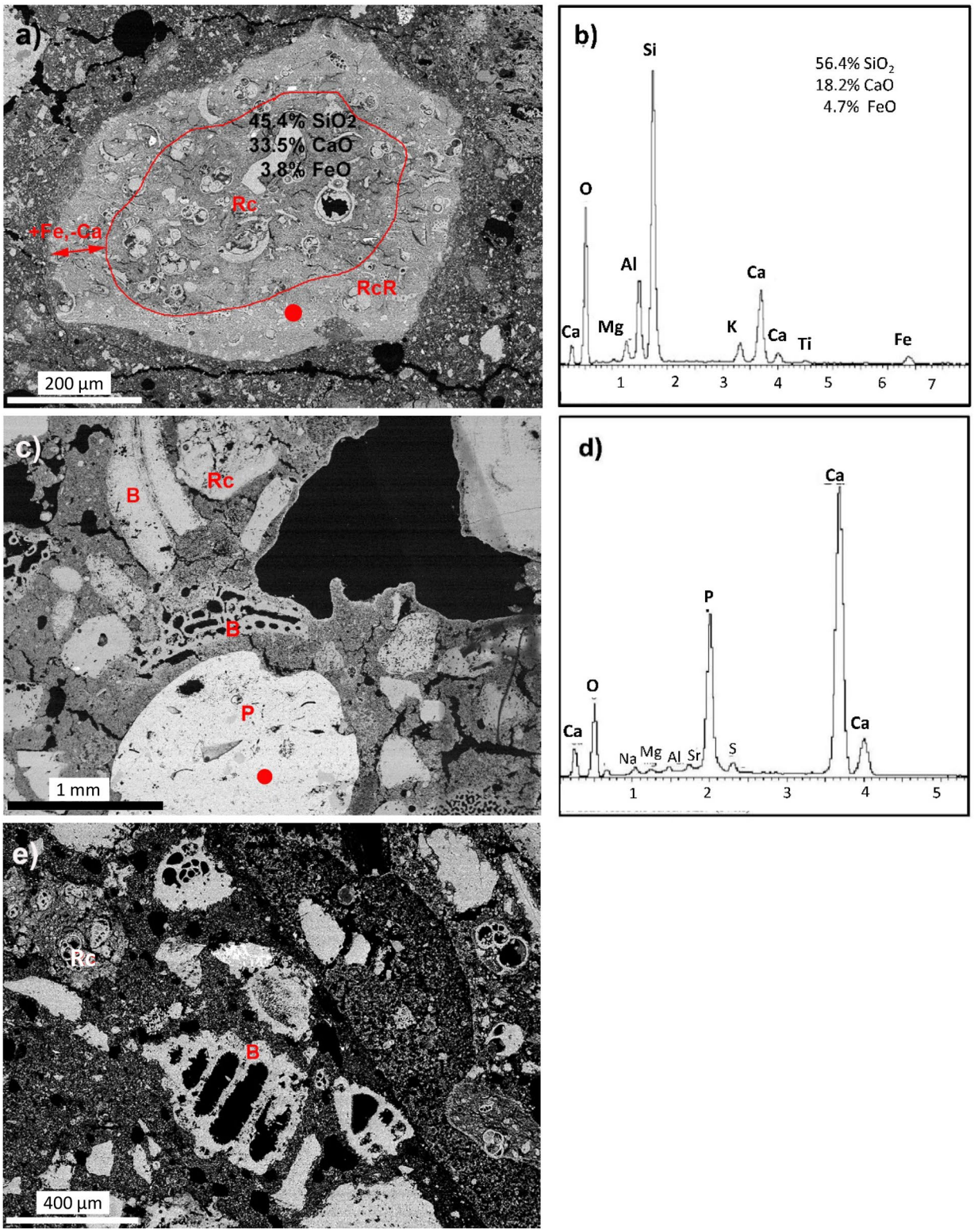

Fig. 5 **a** SEM-BSE images and **b** point analysis EDS of mortar Type 1 (MA-1). Rc: marl fragment with rubefacted edge and microfossils fragments in its interior. **c** SEM-BSE images and **d** point analysis EDS of mortar Type 2 with marl fragments (Rc) and bioclasts (B) (MA-19C) and grain rich in calcium phosphate (P). **e** SEM-BSE images and b point analysis EDS of mortar Type 3 (MA-2A) with bioclasts (B) and marl fragments (Rc). Red point: analysis EDS

a ceramic matrix composed of 17–19% CaO and 5–10% FeO, and contains voids left by dissolved bioclasts (globigerinae), in addition to quartz and K-feldspar grains. The second type is more compact and less porous, with a highly fissured matrix, and consists of < 7% CaO and > 7% FeO. There are frequent grains of quartz and K-feldspar which are < 0.125 mm in size.

The great heterogeneity of the aggregates of this type of mortar is reflected in their varied mineralogical (PLM-XRD) and chemical (EDS) composition. Although calcite dominates, the presence of clay minerals, quartz, and hematite associated with the marls, as well as rubefacted marls and ceramic fragments, are significant (Fig. 5a, b). The binder surrounding these aggregates is a dense and microcrystalline mass and green–brown colour (Fig. 4b). The chemical composition of the binder is quite variable (Fig. 7). Only one sample was found with a pure calcitic binder (100% CaO, MA-19B). In the remaining samples, the binders have a high content of SiO_2-Al_2O_3-FeO, which varies from 22 to 53%, whereas the CaO content is here 44–83%. The porosity, which can exceed 15–20%, is of the vacuolar, fissure, moldic, and intragranular varieties. The first two occur in the binder; the latter two types are associated with fossil remains in limestone and marl fragments.

Type 2: mortars with limestone and bioclast fragments (samples MA-2B, MA-4, MA-6, MA-18B, MA-19C, MA-20, MA-23).

This group consists of mortars which are white to beige in colour, homogeneous in composition, well sorted, and finer textured in appearance than the Type 1 mortars (Fig. 4c). The aggregate/binder ratio is estimated at 4:1 to 3:1. There are two types of aggregates, with 1:1 ratio. The first are whole or fragmented bioclasts (Fig. 4d) between 100 µm (micro-foraminifera: *Globigerina*) and 2 mm (gastropods, echinoderms, bryozoans, brachiopods, and bivalves) in size. These retain their original fibrous-lamellar texture consisting of aragonite and/or calcite (100% CaO) and magnesian calcite (> 92% CaO, > 7% MgO). In the second type, there are sub-rounded fragments of limestone (> 90% CaO) and marl (> 79% CaO and > 20% SiO_2-Al_2O_3-K_2O) (Figs. 4d, 5c, and 6a) with bioclasts (*Globigerina*), ranging from mudstones to packstones (Dunham 1962). Like Type 1, this mortar type also contains some rubefacted grains. The presence of some grains of calcium phosphate or hydroxyapatite (> 52% CaO and > 34% P_2O_5) is also noteworthy (Fig. 5c, d). The binder is a brown microcrystalline mass (Fig. 4d), and it has a mainly calcitic composition. The CaO content of these binders (Fig. 7) varies from 99.8 (MA-19C) to 79% (MA-2B), with a very low content of SiO_2-Al_2O_3-FeO (< 19%). The fissure-type of porosity within these binders is very evident; some vacuolar porosity is also present. Intragranular porosity, which exceeds 10–15%, occurs within the limestone and

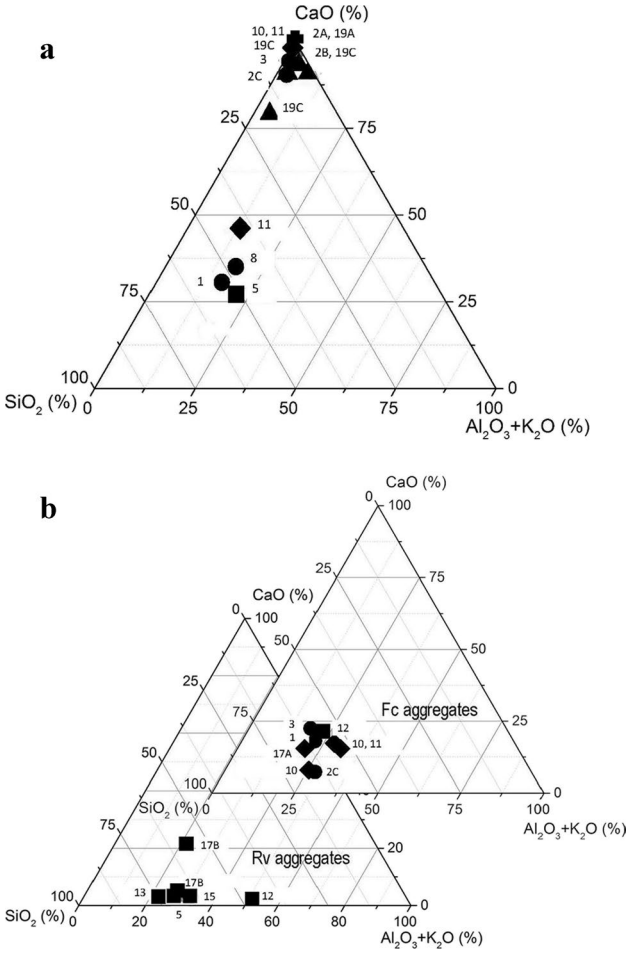

Fig. 6 **a** SiO_2-CaO-($Al_2O_3 + K_2O$) ternary phase diagram of carbonate fragments. Classification according to shape, Circle: Type 1. Triangle: Type 2. Cross: Type 3. Rhombohedron: Type 4. Square: Type 5. **b** SiO2-CaO-(Al2O3 + K2O) ternary phase diagram of volcanic rock aggregates (Rv) and ceramic fragments (Fc). Classification according to shape, Circle: Type 1. Rhombohedron: Type 4. Square: Type 5

marl fragments. In summary, the Type 2 mortars are similar to Type 1, except for the presence of bioclasts and for the fact that the size of the aggregates does not exceed 2 mm. It is also necessary to note the markedly lower content of SiO_2-Al_2O_3-FeO in Type 2 binders, compared to the higher percentages seen in the Type 1 binders.

Type 3: mortars with bioclast fragments (samples MA-2A, MA-18A, MA-19A, MA-22A, MA-24A).

All the samples of this group come from the outer layers of painted wall renders (1.5–3.0 mm thick), except for two samples (MA-18A and MA-24A) that make up the inner layers of non-painted wall renders (Figs. 4e and 8). These are characterised as being very white, compact, cohesive, and fine texture. They also always occur as a plaster layer above

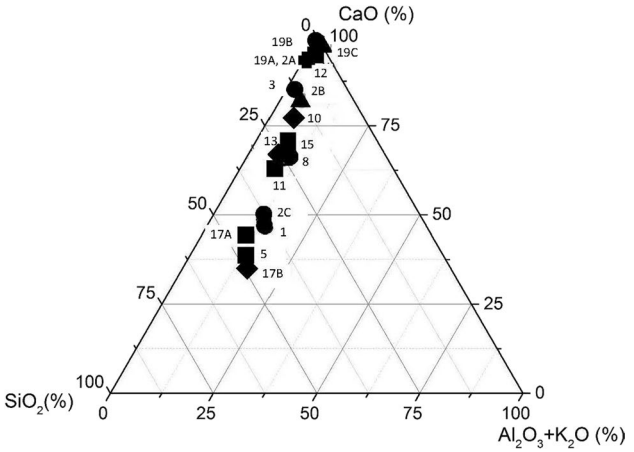

Fig. 7 SiO_2-CaO-($Al_2O_3 + K_2O$) ternary phase diagram of binder. Classification according to shape, Circle: Type 1. Triangle: Type 2. Cross: Type 3. Rhombohedron: Type 4. Square: Type 5

mortars which have aggregates of fossiliferous limestone fragment characteristic of Types 1 and 2 (Fig. 8). These renders show aggregate/binder ratio ranging from 3:2 to 2:1. The aggregates used in these mortars are bioclastic grains consisting of microforaminifera (uniserial and biserial globigerinae) and angular fragments of bivalves, echinoderms, bryozoans, coralline algae, gastropods, and brachiopods, with sizes < 0.5 mm (Figs. 4f and 5e). These aggregates show a CaO content of more than 90% (Fig. 6a). These bioclasts retain their original texture of aragonite or calcite. There are also some grains of limestone and marl with globigerinae. The binder (Figs. 4f and 8) is a dense, dark, and microcrystalline mass of calcite whose chemical composition is > 92% CaO and < 7% SiO_2-Al_2O_3-FeO (Fig. 7). These mortars have a low porosity (< 5%).

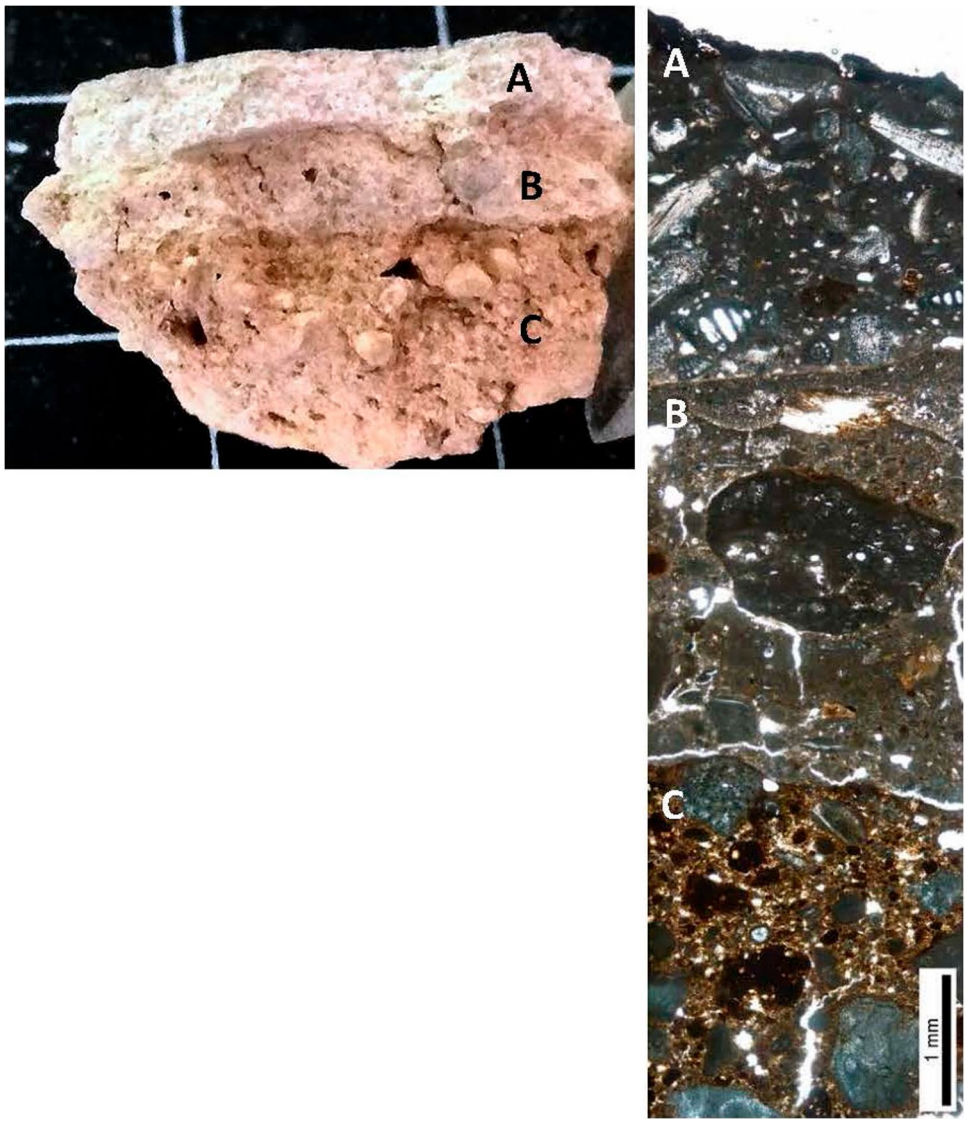

Fig. 8 Visual and PLM (parallel polarised light mode) images of three layered rendering mortar of wall painting (MA-2). Lower layer (**C**) is hydraulic lime mortar with marl/limestone and rubefacted marl fragments (Type 1). Intermediate layer (**B**) is hydraulic mortar with marl/limestone fragments and bioclasts (Type 2), and higher layer (**A**) is aerial lime mortar with bioclast fragments (Type 3)

Type 4: mortars with ceramic fragments (samples MA-10, MA-11, and MA-17B).

This group consists of pinkish mortars and a very cohesive matrix (Fig. 4g). They contain sub-angular aggregates, which are heterogeneous in composition, poorly sorted (grain sizes < 4 mm) and represent more than 60% of the bulk of the mortar (Fig. 4h) with an estimated aggregate/binder ratio of 3:2. These aggregates are of two types. The first type is dominated by ceramic fragments that display varying degrees of vitrification (Fig. 4h); the other contains limestone and marl fragments with preserved globigerinae. Both the latter components are similar to those occurring in Types 1 and 2 mortars. The ceramic fragments are also of two types (Fig. 9a, b). The first is characterised by abundant porosity (irregular and moldic pores), a vitreous paste, and a chemical composition consisting of CaO (15–18%), SiO_2 (> 54%), and Al_2O_3 (> 20%) (Fig. 6b). Within these fragments, there are grains consisting of clay minerals, quartz, K-feldspars, and calcium phosphate (hydroxyapatite; CaO 50.2%, P_2O_5 42%), as well as Fe-Ti, Fe-Ca and CaO grains, and other ceramic fragments. The molds within the ceramic fabric have been formed by impressions of globigerinae or other microforaminifera destroyed during firing. In the second group of ceramic fragments, *Globigerina* with their original preserved shells (100% CaO), quartz, K-feldspars, and calcium phosphate grains are present. The clayey matrix of these ceramic fragments is more abundant than in the previous type, and there is less CaO (< 8%) and Al_2O_3 (< 20%) and more SiO_2 (> 66%) (Fig. 6b). The texture is uneven, due to mixing of the original ceramic fragments, and is also less vitrified, highly dense, and less porous (however exhibiting fissures and intragranular porosity).

The second type of aggregate consists of limestone (> 96% CaO) and marl (> 46% CaO and > 53% SiO_2-Al_2O_3-K_2O) fragments (Figs. 4h and 6a) that can be attributed to a mudstone to packstone facies, as determined by the bioclastic content (5 to > 60%). There are also some isolated bioclast fragments (< 5%), rubefacted marl, and limestone grains. Sample MA-17B contains only ceramic fragments as aggregates and decomposed plant remains.

The binder is a dense microcrystalline mass and contains dispersed iron amorphous masses due to ceramic dust, which gives it a pink colour. The chemical composition of these binders shows a high SiO_2-Al_2O_3-FeO content, ranging from 24–34% in samples MA-10 and MA-11 and up to almost 62% in sample MA-17B (Fig. 7). The porosity of these mortars is around 10–15% (fissure, vacuolar, and intragranular porosities).

Type 5: mortars with volcanic rock fragments (MA-5, MA-7, MA-12, MA-13, MA-14, MA-15, MA-16, MA-17A, MA-21).

The mortars in this group are characterised as lightweight, porous, low-cohesion grey mortars, with abundant (> 60%) angular and sub-angular aggregates (Fig. 4i) and a grain size of < 2 mm. The aggregate/binder ratio for this mortar type is approximately 3:2. One of these samples (MA-7) contains aggregates having a large size range (8–16 mm). Most (80%) of these aggregates consist of volcanic fragments with trachytic, vitreous, vesicular, and porphyritic textures and monomineralic grains (Figs. 4j and 9c, d). The mineralogical and chemical composition of these volcanic fragments (Fig. 6b) indicates that they are mainly from sanidine-rich trachyte and andesite rocks (alkali feldspars consisting of 3–4.5% Na_2O, 7–9% K_2O, 17–21% Al_2O_3, 60–65% SiO_2, 0.6–0.9% MgO, 2–3% CaO, 2–4% FeO, and 0.4–0.6% TiO_2). The monomineralic grains appear as prismatic phenocrysts within the volcanic fragments or as isolated prismatic crystals in the binder (Fig. 9c, d); these are composed mainly of plagioclases (mainly sanidine and andesine) and pyroxenes (augite).

Making up a smaller percentage of the aggregate (5–15%) are limestone and marl fragments containing globigerinae (mudstone to packstone; > 99% CaO), ceramic fragments, rubefacted marl grains, and black particles (< 100 µm), which derive probably from calcination (residual ash) or volcanic activity (volcanic ash). In addition, there are a few lime lumps of incompletely calcined carbonate rock (5–10%) having a chemical composition of approximately 92% of CaO and 7% of SiO_2-Al_2O_3; these are up to 3 mm in size and have high fissure internal porosity due to shrinkage during the hardening process of the mortars.

The binder shows a dark, greenish-brown, microcrystalline mass with a mainly calcitic composition (Fig. 4j). It also contains some amorphous iron inclusions and has a vacuolar porosity (5–10%). The binder composition falls within a range of 28–61% of SiO_2-Al_2O_3-FeO. The binders of samples MA-5 and MA-17A have the highest concentrations of SiO_2-Al_2O_3-FeO (55–61%) compared to CaO (36–42%). In contrast, the binders of samples MA-13 and MA-15 have high CaO concentrations (65–69%) and in the case of sample MA-12 > 94% CaO (Fig. 7).

Hydraulicity based on TGA–DSC analysis

Figure 10 shows the relation between the reverse trend of the degree of hydraulicity (CO_2/H_2O) and the CO_2 ratio of the samples; this trend increases exponentially (Moropoulou et al. 2005; Genestar et al. 2006), where the samples having values below 10 on the *y*-axis of this graph can be considered hydraulic binders (Moropoulou et al. 2000; Genestar et al. 2006; Uğurlu Sağın et al. 2021). The samples which are located in (CO_2/H_2O) below 5 and CO_2 below 20% are considered highly hydraulic binders (Moropoulou et al. 2005).

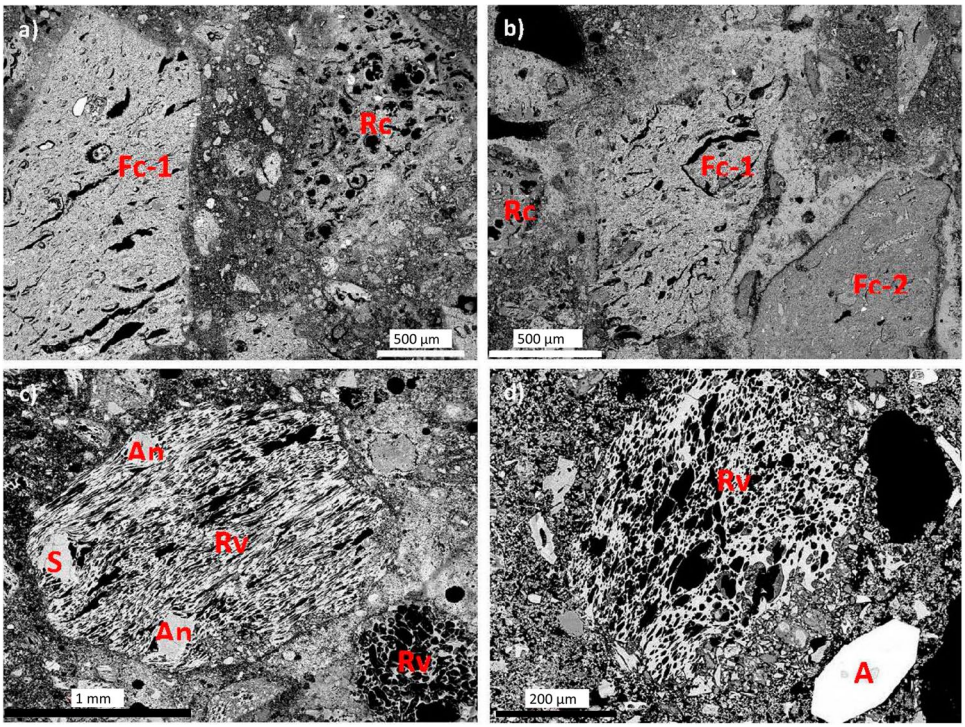

Fig. 9 SEM-BSE images of **a** Type 4 mortar MA-11 and **b** Type 4 mortar MA-10 with the presence of two types of ceramic fragments (Fc) and some microfossiliferous marl fragments (Rc). The Fc-1 fragments have more porosity and higher Ca content than Fc-2. SEM-BSE images of **c** Type 5 mortar MA-13 with volcanic fragments (Rv) and isolated minerals as the main aggregate. The mineralogy of Rv is sanidine and the phenocrysts it contains are andesine (An) and sanidine (S). **d** Type 5 mortar MA-15 with volcanic fragments (Rv) of sanidine and with isolated minerals of augite (clinopyroxenes)

Type 1 mortars exhibit a wide range of weight loss (Table 3). Losses ranging from 1 to 8% are due to the release of hygroscopic water (< 120 °C) and dehydration of hydrated salts and hydraulic components (C-S–H/C-A-H/C-A-S–H) (120–200 °C) at temperatures below 200 °C, bound H_2O content in hydraulic compounds calcium silicate hydrate/calcium aluminate hydrate/calcium aluminium silicates hydrates (C-S–H/ C-A-H/ C- A—S–H), clay dehydroxylation (200–600 °C) which ranges between 2 and 6%, and 17–39% weight loss attributed to the release CO_2 due to the decomposition of carbonate minerals when heated above 600 °C. Additional exothermic peaks in DSC curves after 800 °C which show the decomposition of carbonate as aggregate are detected in MA-9 sample in Type 1. This type of mortar has a high variability in the CO_2/H_2O ratio, of between 3 and 15 (Fig. 10).

Types 2 and 3 are similar, with little weight loss evident below 200 °C (0.5–2.7%) and between 200–600 °C

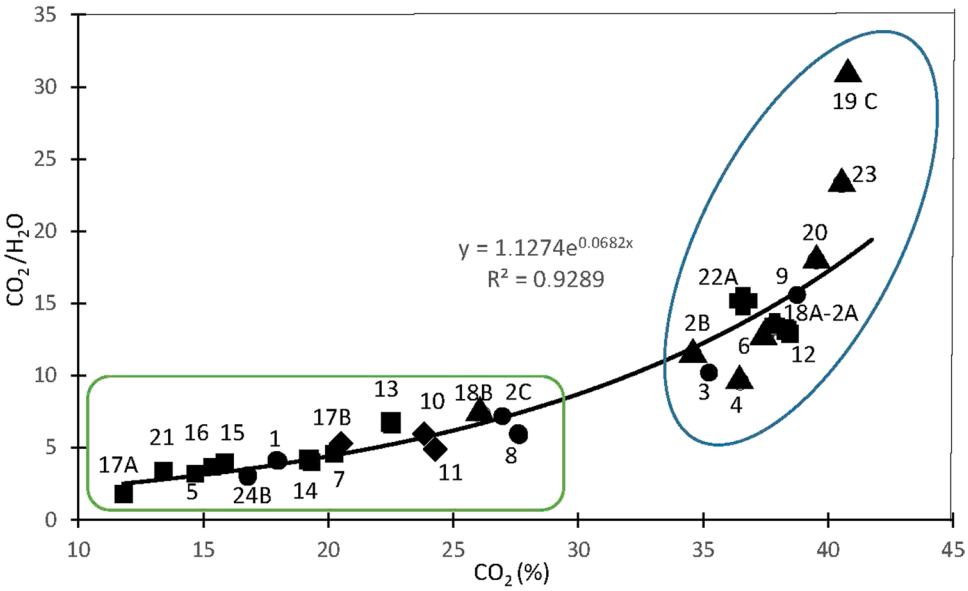

Fig. 10 Graph CO_2/H_2O vs CO_2 (%) useful to classify the mortars; CO_2/H_2O‹10 indicate the hydraulic character, so the mortars above 10 with higher CO_2 amounts can be discarded as the non-hydraulic true lime mortars; the others indicate hydraulic character of the lime and among those so-called hydraulic lime mortars. Classification according to shape, Circle: Type 1. Triangle: Type 2. Cross: Type 3. Rhombohedron: Type 4. Square: Type 5

Table 3 Mass losses (%) gathered in thermal analysis (TGA)

Type Mortar	Samples	< 120°C	120-200°C	200-600°C	> 600°C	CO_2/H_2O	Hydraulicity
Type 1	MA-1	3.49	1.55	4.34	17.99	4	HH
	MA-2C	2.03	0.38	3.74	26.96	7	H
	MA-3	1.41	0.42	3.47	35.23	10	NH
	MA-8	2.2	1.27	4.69	27.63	6	H
	MA-9	0.78	0.24	2.48	38.75	16	NH
	MA-24B	5.99	1.66	5.52	16.77	3	HH
Type 2	MA-2B	1.35	0.27	3.00	34.57	12	NH
	MA-4	1.36	0.58	3.79	36.47	10	NH
	MA-6	0.97	0.24	2.93	37.48	13	NH
	MA-18B	0.93	0.34	2.78	37.85	14	NH
	MA-19C	0.39	0.1	1.33	41.77	31	NH
	MA-20	0.88	1.75	2.20	39.52	18	NH
	MA-23	0.67	0.00	1.74	40.54	23	NH
Type 3	MA-2A	1.07	0.32	2.81	37.78	13	NH
	MA-18A	2.34	0.37	3.58	26.14	7	H
	MA-22A	1.17	0.00	2.38	36.52	15	NH
Type 4	MA-10	2.25	0.85	4.02	23.85	6	H
	MA-11	2.63	1.08	4.92	24.34	5	H
	MA-17B	5.44	2.66	6.62	11.8	2	HH
Type 5	MA-5	2.9	1.21	4.59	14.67	3	HH
	MA-7	2.32	0.93	4.38	20.23	5	HH
	MA-12	0.89	0.3	2.98	38.46	13	NH
	MA-13	1.55	0.68	3.41	22.55	7	HH
	MA-14	2.31	0.92	4.84	19.32	4	HH
	MA-15	3.05	1.27	4.01	15.85	4	HH
	MA-16	3.11	1.39	4.12	15.34	4	HH
	MA-17A	2.82	1.09	4.05	20.33	5	H
	MA-21	4.98	0.00	3.91	13.4	3	HH

HH high hydraulic, *NH* non hydraulic, *H* hydraulic

(1–4%); however, the loss becomes more significant above 600 °C (34–42%), which indicates a higher carbonate content. These also have the highest CO_2/H_2O ratios (between 10 and 31). All samples can be regarded as non-hydraulic binders except one sample (MA-18A) in Type 3 has a lower carbonate component (26.1%) and higher weight loss associated with release of adsorbed moisture and water related to hydrated compounds below 120 °C (Table 3).

Mortar types 4 and 5 are quite similar to each other in hydraulicity. Each has a relatively high weight loss below 200 °C (3–8%), between 200 and 600 °C (3–7%), and a lower loss above 600 °C (12–24%) when compared to the previous types of mortars, and accordingly has the lowest CO_2/H_2O ratio between 1.8 and 6. The MA-12 mortar shows incongruous values, with low weight loss between 200 and 600 °C (3%) and very high loss above 600 °C (38%). The CO_2/H_2O ratio is high. Type 4 mortars have binders with hydraulic properties, and binders of Type 5 mortars show a highly hydraulic nature, except for MA-12.

Chemical analysis by XRF on bulk sample

Analyses of the whole samples carried out by XRF show a number of differences mainly due to the range of aggregate types present in each mortar group (Tables 4, 5; Fig. 11). Similarly to the TGA/DCS analyses, three clusters are detected. Mortars with mostly carbonate aggregates (bioclastic fragments and fossiliferous limestone and marl fragments) have a higher CaO content (Types 1, 2, and 3: 35–66%), with percentages averaging 52–61% (Tables 4, 5). Of these three types, Type 1 mortars are somewhat distinct from the others, as they display a greater compositional heterogeneity with higher concentrations of SiO_2 (5–19%), Al_2O_3 (1.5–5.4%), K_2O (0.2–0.8%), and Fe_2O_3 (0.3–2.9%), due to the presence of silicate minerals within fragments of marls, rubefacted marls, and ceramics. Mortars with primarily fragments of bioclasts (Types 2 and 3) have a more homogenous, CaO-rich composition (56–64% CaO) with lower concentrations of SiO_2 (0.9–7%), Al_2O_3 (0.2–2.2%), K_2O (0.1–0.3%), and Fe_2O_3 (0.2–0.7%).

Mortars rich in marl fragments (Types 1 and 2) also have a higher P_2O_5 content. Types 4 and 5 mortars have the lowest CaO percentages (26–47%) and the highest concentrations of SiO_2 (15–43%), Al_2O_3 (2–10.5%), K_2O (0.7–3.7%), and Fe_2O_3 (1.8–2.8%). Mortars with ceramic aggregates (Type 4) have a CaO content (46%) which is greater than the CaO content (33%) for mortars rich in volcanic-type aggregates (Type 5); the latter mortars also show an increase in the presence of other elements such as K_2O (1–3.7%), due to a greater concentration of Na–K feldspars (plagioclases and sanidine). As with TGA/DCS analyses, there are outliers—in this case, these are samples MA-18B and MA-12. The first sample (Type 2, MA-18B) shows clear anomalies, with high concentrations of SiO_2 (17%), Al_2O_3 (6.7%), K_2O (0.6%), Fe_2O_3 (0.9%), and P_2O_5 (1.1%). This sample contains more fragments of marls and phosphatic grains than limestone fragments, which are generally dominant in other Type 2 mortars. The second anomalous sample (Type 5, MA-12) has a very high concentration of CaO (64%) and relatively low concentrations of the rest of the chemical components—this sample also shows a great compositional heterogeneity of its aggregate, as it has a high concentration of limestone fragments as well as volcanic fragments. The trace element concentrations (Table 6) show that Type 5 mortars, which contain volcanic fragments, contain elements (Bi, Nb, and Rb) not found in the rest of the mortars. On the other hand, Sr and Ba are present within all the five types of mortars; these are elements that are incorporated in the structure of less stable carbonates (i.e., aragonite) and sulfates. Table 5 also presents the concentration means (and standard deviations) of S and Cl of each mortar type. Type 3 mortars stand out, with the lowest concentrations of S and highest of Cl, possibly due to presence of the marine bioclast remains.

Analysis of stable isotopes

Isotopic ratios $\delta^{13}C$ and $\delta^{18}O$ distinguish two different groups of mortars. The Group 1 has a lower concentration of $\delta^{18}O$ that does not usually exceed − 10‰, with a $\delta^{13}C$ ranging between − 12.3 and − 7.2‰; the Group 2 shows greater variation, with a maximum concentration of $\delta^{18}O - 3‰$ and with $\delta^{13}C$ ranging between − 17.5 and − 4.5‰ (Fig. 12). Both groups have a $\delta^{13}C/\delta^{18}O$ ratio defined by the following lines of regression:

Group 1: $\delta^{18}O = 0.611\ \delta^{13}C - 1.4728$ $R.^2 = 0.75$
Group 2: $\delta^{18}O = 0.828\ \delta^{13}C - 3.3355$ $R.^2 = 0.74$

In both mortar groups, a trend of continuous enrichment of $\delta^{13}C$ and $\delta^{18}O$ is observed. The mortars of Group 1 contain aggregates dominant in limestone and marl fragments (Type 1). The Group 2 contains Type 2 mortars and plasters with bioclasts (Type 3). Mortars with natural pozzolanic aggregates (Type 5) or artificial pozzolanic aggregates (Type 4) are located on both trend lines, with lower values of $\delta^{13}C/\delta^{18}O$. The mortar of the intermediate layer of sample 2 (MA-2B) is placed in Group 1 and corresponds to an isotopic fractionation which follows the trend observed in Type 1 mortars. In contrast, the MA-3 mortar, which contains limestone fragments, is found in Group 2. Apart from these two atypical samples, the rest of the mortars are grouped within the trends indicated.

Discussion

This characterisation study of the binders and aggregates of the mortars and plasters used at the Żejtun Villa has allowed us to distinguish five distinct groups. All five mortar types contain as aggregate limestone and marl fragments, rich in bioclasts (globigerinae), probably originating from the *Globigerina* Limestone Formation of Miocene age in Malta (Foresi et al. 2014; Baldassini and Di Stefano 2017). This suggests that the local geology played an important role in the making of these mortars (Degryse et al. 2002; Ergenç and Fort 2019). The high concentrations of planktonic microforaminifera, as well as of rubefacted and phosphatised grains, could have originated from the hardground facies present in the lower part of this geological formation (Foresi et al. 2014; Baldassini and Di Stefano 2017). This implies a potential extraction point for these raw materials within the upper part of the lower member and/or the lower part of the middle member of this geological formation.

These carbonate aggregates especially dominate in Types 1 and 2 of the mortars, which include samples usually present at the inner (or middle) layer of wall plasters. In Type 1 mortars, the dominant aggregates are CaO-depleted (clayey and rubefacted) marl fragments (< 32%) and binders that have a lower CaO content (44–83%), whilst in Type 2 mortars, the dominant aggregates are CaO-rich limestone fragments (> 80%), and binders also have high CaO contents (79–100%).

This is reflected in their hydraulicity, with Type 1 mortars being more hydraulic than Type 2 mortars (Tables 2 and 3; Fig. 10), because the aggregates (clayey and rubefacted marls) give additional hydraulicity to the mixtures, according to Moropoulou et al. (2005). The highly hydraulic nature of samples MA-1, MA-24B, and hydraulic nature of MA-8 are also observed on DSC curves and moisture content (Table 3).

The aggregates composed of aragonite, calcite, and Mg-calcite bioclasts (> 90% in CaO and Sr and Mg traces; EDS), which appear mainly in Types 2 and 3 mortars, belong to benthonic marine organisms of the Quaternary period,

Table 4 Chemical composition of the mortar samples grouped according to their types

Sample	% CaO	% SiO_2	% Al_2O_3	% K_2O	% Fe_2O_3	% P_2O_5	% TiO_2	S (ppm)	Cl (ppm)
Type 1								Type 1	
MA-1	55.10 ± 0.33	7.81 ± 0.11	2.93 ± 0.26	0.23 ± 0.01	1.08 ± 0.01	0.34 ± 0.10	0.20 ± 0.01	2370 ± 111	220 ± 25
MA-2C	43.07 ± 0.13	19.32 ± 0.11	5.38 ± 0.06	0.76 ± 0.02	2.30 ± 0.02	0.54 ± 0.15	0.36 ± 0.01	1840 ± 115	410 ± 15
MA-3	55.78 ± 0.17	7.67 ± 0.11	2.27 ± 0.11	0.19 ± 0.02	0.55 ± 0.00	0.54 ± 0.07	0.18 ± 0.01	4100 ± 189	2070 ± 61
MA-8	61.91 ± 0.38	4.58 ± 0.04	2.04 ± 0.37	0.18 ± 0.02	0.34 ± 0.00	0.24 ± 0.08	0.20 ± 0.01	2850 ± 90	900 ± 6
MA-9	57.97 ± 0.47	5.56 ± 0.10	1.53 ± 0.08	0.19 ± 0.02	0.60 ± 0.01	0.31 ± 0.05	0.20 ± 0.02	1630 ± 44	180 ± 17
MA-24B	34.74 ± 0.26	14.74 ± 1.09	4.78 ± 0.51	0.58 ± 0.28	2.85 ± 0.22	0.27 ± 0.02	0.33 ± 0.10	3190 ± 100	3080 ± 615
Type 2								Type 2	
MA-4	62.54 ± 0.51	4.85 ± 0.11	1.04 ± 0.17	—	0.41 ± 0.01	0.21 ± 0.02	0.20 ± 0.02	2230 ± 35	300 ± 0
MA-6	63.95 ± 0.96	5.00 ± 0.10	2.04 ± 0.21	0.09 ± 0.00	0.41 ± 0.01	0.29 ± 0.09	0.22 ± 0.00	1960 ± 75	630 ± 21
MA-18B	57.94 ± 0.56	17.10 ± 0.24	6.67 ± 0.12	0.55 ± 0.02	0.94 ± 0.02	1.06 ± 0.07	0.33 ± 0.01	2060 ± 72	390 ± 30
MA-19C	65.82 ± 0.50	5.16 ± 0.16	2.17 ± 0.16	0.13 ± 0.02	0.23 ± 0.00	0.24 ± 0.08	0.22 ± 0.01	2090 ± 42	230 ± 35
MA-20	55.58 ± 2.18	6.98 ± 2.34	0.90 ± 0.31	0.23 ± 0.01	0.48 ± 0.04	0.31 ± 0.08	0.09 ± 0.01	3028 ± 1670	17,340 ± 1117
MA-23	57.96 ± 1.36	0.90 ± 0.01	0.25 ± 0.04	0.10 ± 0.03	0.24 ± 0.04	—	0.09 ± 0.01	160	560 ± 21
Type 3								Type 3	
MA-22A	57.50 ± 0.36	4.84 ± 0.04	0.83 ± 0.16	0.26 ± 0.01	0.70 ± 0.02	0.18 ± 0.01	0.14 ± 0.01	1007 ± 50	1727 ± 23
Type 4								Type 4	
MA-10	44.61 ± 0.28	20.77 ± 0.20	7.05 ± 0.60	0.77 ± 0.01	2.79 ± 0.04	0.66 ± 0.07	0.46 ± 0.00	1720 ± 36	430 ± 35
MA-11	46.78 ± 0.13	24.48 ± 0.30	7.60 ± 0.37	0.73 ± 0.07	2.60 ± 0.01	—	0.42 ± 0.01	2310 ± 15	190 ± 35
Type 5								Type 5	
MA-5	22.97 ± 0.18	38.64 ± 0.40	8.17 ± 0.32	2.35 ± 0.02	2.38 ± 0.03	0.47 ± 0.02	0.28 ± 0.01	5760 ± 144	1390 ± 0
MA-7	23.93 ± 0.28	40.64 ± 0.81	10.21 ± 0.41	3.70 ± 0.08	2.57 ± 0.01	0.27 ± 0.08	0.32 ± 0.01	850 ± 36	3090 ± 102
MA-12	63.70 ± 0.18	2.30 ± 0.15	0.99 ± 0.16	0.08 ± 0.01	0.28 ± 0.01	—	0.20 ± 0.00	1430 ± 50	1970 ± 49
MA-13	36.90 ± 0.26	22.80 ± 0.20	5.05 ± 0.10	1.33 ± 0.03	1.77 ± 0.04	—	0.24 ± 0.01	1280 ± 59	760 ± 65
MA-14	32.83 ± 0.03	31.47 ± 0.36	7.86 ± 0.30	2.22 ± 0.01	2.11 ± 0.01	0.71 ± 0.04	0.30 ± 0.00	3080 ± 160	1100 ± 55
MA-15	27.61 ± 0.35	28.35 ± 0.33	6.04 ± 0.09	1.90 ± 0.05	2.16 ± 0.02	0.32 ± 0.11	0.26 ± 0.01	3640 ± 38	540 ± 25
MA-16	25.76 ± 0.34	38.17 ± 0.83	10.30 ± 0.49	2.01 ± 0.05	2.54 ± 0.02	0.38 ± 0.06	0.31 ± 0.01	3480 ± 26	560 ± 10
MA-17A	28.39 ± 0.08	43.20 ± 0.47	10.49 ± 0.44	1.85 ± 0.02	2.04 ± 0.00	—	0.32 ± 0.01	3090 ± 93	790 ± 50
MA-21	38.34 ± 1.69	14.85 ± 1.52	1.96 ± 0.42	1.04 ± 0.21	2.75 ± 0.23	1.35 ± 0.05	0.24 ± 0.03	3217 ± 310	480 ± 44

Table 5 Mean and standard deviation of major elements of different type of mortars

Type	% CaO	% SiO_2	% Al_2O_3	% K_2O	% Fe_2O_3	% P_2O_5	% TiO_2	S (ppm)	Cl (ppm)
1	51.43 ± 10.33	9.95 ± 5.81	3.16 ± 1.57	0.36 ± 0.25	1.29 ± 1.04	0.37 ± 0.13	0.25 ± 0.08	2663 ± 917	1143 ± 1182
2	60.63 ± 4.04	6.67 ± 5.49	2.18 ± 2.32	0.22 ± 0.19	0.45 ± 0.26	0.42 ± 0.36	0.19 ± 0.09	2274 ± 433	422 ± 170
3	57.50	4.84	0.83	0.26	0.70	0.18	0.14	1007	1727
4	45.70 ± 1.54	22.63 ± 2.62	7.33 ± 0.39	0.75 0.03 ±	0.69 ± 0.13	0.33	0.44 ± 0.03	2015 ± 417	310 ± 170
5	33.38 ± 12.60	28.93 ± 13.57	6.79 ± 3.56	1.83 ± 0.99	2.07 ± 0.74	0.59 ± 0.41	0.27 ± 0.04	2965 ± 855	705 ± 230

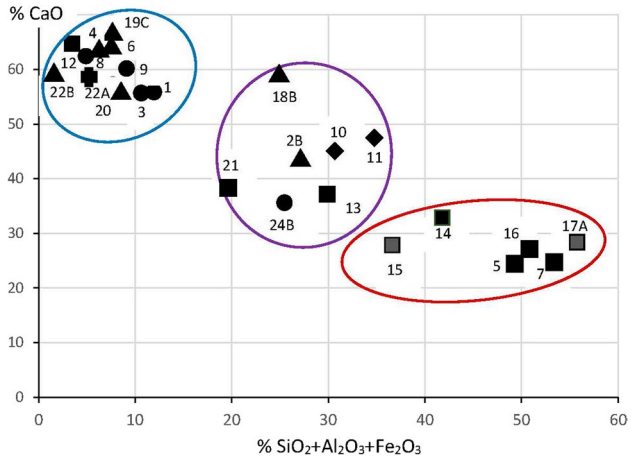

Fig. 11 Chemical composition of the whole mortar samples. Classification according to shape, Circle: Type 1. Triangle: Type 2. Cross: Type 3. Rhombohedron: Type 4. Square: Type 5

possibly obtained from a local beach. Besides, mortars with bioclasts are those with the highest chloride content (probably from marine salt) (Table 4). The highest weight loss between 120 and 200 °C in thermal analysis was also detected in MA-20 (Table 3).

The geologic time of those mortars could be determined by bioclastic materials since they retain its original, mineralogical textures, and composition, which unstable polymorph aragonite and magnesian calcite transform into stable calcite during geologic burial and subsequent fossilisation (Noel and Brian 2016).

The binders of Type 3 mortars are also high in CaO (> 92%; EDS). This is reflected in the thermogravimetric and chemical analyses (Table 3, Figs. 6a, 7, 10, and 11). The characteristics of these aerial lime mortars explain their use for the external layers of wall renders, on Types 2 and 3 mortars. This is an observation even made by ancient Roman architect and writer Marcus Vitruvius (Morgan 1960) and confirmed locally by Deguara (2015). Nevertheless, wall render sample MA18, which is the outer layer of sample MA 18A (Type 3), appears to have a greater hydraulic nature than the inner layer MA-18B, of the same composite sample (Type 2) (Table 3, Fig. 10). This discrepancy can be explained by the possible non-deliberate use of rubefacted marl in binder preparation for the uppermost layer. Alternatively, if the same binders were used in both layers, the difference would be in the reaction products of marly aggregates and binder included in the enriched binder sample of the outer layer.

The compositional analyses and the perceived function of the samples of Type 1, 2, and 3 show a broad range of mortar mixtures, based mostly on the local availability of raw materials in the Early Roman period. Also, the aggregate/binder ratios differ in each type of mortar, with the presence of binder being more abundant in the Type 3 exterior mortar (40–50%) and less in the Type 2 interior mortar (20–25%). The binders of these mortars appear to originate from the same limestone deposits, which also contain marls (impure limestones with clays) rich in globigerinae and hardgrounds, and that the Romans used as aggregates, possibly explaining why the lime binders have different hydraulic degrees.

For the sake of accuracy, superimposition of the results coming from the TGA/DSC analyses should also be considered. The H_2O mass loss between 200 and 600 °C can be attributed to hydraulic phases which can be both calcium silicate and aluminate hydrates (CSH and CAH, respectively) or due to the marly nature of binder. Note that clays may dehydroxylate at various temperature ranges such as 300–550 °C 500–650 °C, 480 °C, 520 °C, 580 °C,

Table 6 Mean and standard deviation of trace elements of different type of mortars

Type	Ba	Bi	Cr	Mn	Nb	Pb	Rb	Sr	Zn	Zr
1	205 ± 41	—	78 ± 18	165 ± 78	—	20 ± 0	—	318 ± 127	32 ± 14	51 ± 24
2	167 ± 32	—	75 ± 10	—	—	—	—	191 ± 94	—	—
3	160	—	—	—	—	—	—	223	20	27
4	250 ± 90	—	125 ± 21	—	—	—	—	290 ± 57	45 ± 7	80 ± 14
5	317 ± 54	26 ± 5	80 ± 20	476 ± 76	32 ± 21	30 ± 0	52 ± 10	276 ± 21	46 ± 11	216 ± 41

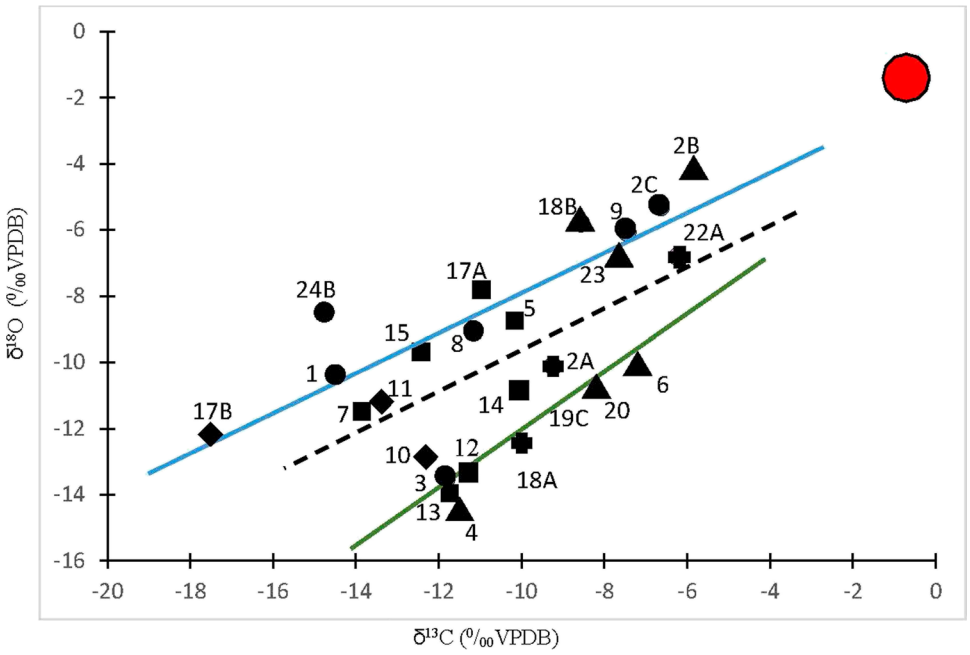

Fig. 12 Regression line of $\delta^{13}C$ vs. $\delta.^{18}O$ of mortars. Blue line: linear regression 1, Green line: linear regression 2, Black dashed line: linear regression of Kosednar-Legensteinetal et al. 2008. Red circle is the isotopic composition of limestones with *Globergina* of intermediate form. Classification according to shape, Circle: Type 1. Triangle: Type 2. Cross: Type 3. Rhombohedron. Type 4. Square: Type 5

and 660–773 °C (Rodriguez-Navarro 2004, Moropoulou et al.1995). There is mass loss between 400 and 600 °C that could be attributed to portlandite, which is also possible to find in historic mortars having experienced various solution and recrystallization processes (Ergenç and Fort 2019); however, no portlandite is detected by XRD. Meta-stable calcium carbonate polymorphs also decompose at 500–600 °C (Morandeau et al. 2014; Ergenç and Fort 2018).

Types 4 and 5 mortars differ from the other mortar types in the aggregate used, but not in the binder type, nor in the aggregate/binder ratio, which is similar to Type 1 mortars (3:2) (Figs. 6b and 7). The main aggregates are in fact siliceous: ceramic fragments in Type 4 and volcanic rock (trachyte and andesite) fragments in Type 5. The ceramic fragments contain the planktonic microforaminifera (globigerininae) prevalent in the local geology of the area and thus clearly indicate local manufacture. The manufacturing of the included ceramics also indicates two different techniques of preparation, as highlighted by their different texture and mineralogical composition. The presence of globigerinae in one type indicates low burning temperature (< 850 °C) whereas their absence together with the presence of a vitrified clayey matrix indicate high firing temperatures (> 850–900 °C). Both these types of aggregates are highly reactive pozzolanic components, giving these mortars extra hydraulicity (Moropoulou et al. 2005). Besides, no volcanic activity occurs on the Maltese Islands, and therefore, the volcanic aggregates do not originate in the Maltese Islands.

Considering the binders of Types 4 and 5, low CaO concentrations (35–42%, Fig. 7) occur in both types (Type 4: MA-17A and Type 5: MA-5 and MA-17B), with a SiO_2-Al_2O_3 + FeO:CaO ratio of 1:1 to 2:1—these are therefore strongly hydraulic.[3] Thermal analyses results also (Table 3, Fig. 10) support the hydraulic degree of Types 4 and 5 binders. It is to be remembered that EDS analysis on binders is influenced by the hydrated products of pozzolanic reactions between lime and ceramic and volcanic fragments and dust (such as ceramic dust in MA-17B). The high hydraulic degree of these two types of mortars not only depends on the use of lean limes with different degrees of hydraulicity (Moropoulou 2005) but also by the type of pozzolan used as aggregate. The only non-hydraulic binder sample of Type 5 (MA12) probably had a lower proportion of crushed volcanic rock aggregate with small particle size.

The binders, which are similar to those used in Type 1 mortars, seem to have been manufactured from the same marly facies.

Mortars sampled from the Żejtun site show that the regression lines (Fig. 12) tend to converge towards higher isotopic fractionation, approaching the values of the *Globigerina* Limestone facies present in outcrops located in the vicinity of the site (Gruszczyńsk et al. 2008).

The presence of marls as the main aggregate in Type 1 mortars (Group 1), together with the presence of limestone fragments, result in an increase in $\delta^{18}O$, thus displacing the trend line as defined by Kosednar-Legenstein (Dotsika et al. 2009).

The isotopic concentrations of the bioclast aggregates in Types 2 and 3 influence the overall isotopic concentrations

[3] This relationship is inverted in another two mortar types (Type 4: MA-10 and MA-11 and Type 5: MA-13 and MA-15), where an increase in CaO content (65–75%) results in ratios of 1:2 and 1:3.

within these mortar types. These shells could suggest that they originated from existing beach deposits in the south-east of the Island. The mean $\delta^{18}O$ values of these shells is + 1.0‰, with a maximum of + 2.1‰ and a minimum of − 0.3‰ (Prendergast et al. 2013).

Two lines mark the isotopic trend line having different negative isotopic values in both lines (Fig. 12). This is possibly related to the water used to mix the mortars, which could have had a different composition, and probably influenced the isotopic composition of the calcite formed during the carbonation and hardening of these mortars. In addition, the oxygen component of the precipitated calcite could have become heavier on evaporation of the water during setting of the mortar (Dotsika et al. 2009). Regression line 2 in Fig. 12, which falls below that established by Kosednar-Legensteinetal et al. 2008, is defined as the transformation of lime ($Ca(OH)_2$) into calcite ($CaCO_3$) induced by atmospheric CO_2 and slightly isotopic meteoric water. The displacement of regression line 1 (Fig. 12), with values of $\delta^{18}O$ between − 13‰ and − 5‰ corresponds to enrichment of the calcite in $\delta^{18}O$ due to the presence of silicate minerals (volcanic rocks and ceramic fragments) and thus indicates that the formation of this calcite is carried out in the presence of atmospheric CO_2 and heavy water evaporation (Dotsika et al. 2018). In addition, hydraulic mortars with a greater chemical reactivity result in the modification of the isotopic content of $\delta^{13}C$ and $\delta^{18}O$ (Toffolo et al. 2020). The increase in $\delta^{18}O$ may be influenced by the presence of saline water (Cangemi et al. 2010; Fort et al. 2021).

The aggregate/binder ratio can also influence the $\delta^{13}C$ content, since high percentages of aggregates or water in the mix can slow down the carbonation process (Van Strydonck et al. 1986). However, our data do not show any relationship between a high lime content and a high aggregate content, coinciding with the observations of Dotsika et al. (2018).

The presence of sulfur (S) and chlorine (Cl^-) identified through chemical analysis illustrate the presence of saline phases. The Żejtun mortar samples were found to have the following mean values: S = 1992 ± 263 ppm and Cl^- = 328 ± 140 ppm. Type 5 mortars that have a higher sulfur and lower chlorine content demonstrate lighter isotope readings in regression line 2 (Fig. 12), so it is possible that the type of salt present in these mortars also influences isotopic fractionation $\delta^{13}C/\delta^{18}O$ (Dotsika et al. 2018; Fort et al. 2021). The MA-3 sample (Type 1), also located on line 2, is the sample with the highest sulfur reading (4100 ppm).

Similarly, Type 3 mortars have the highest Cl^- (1727 ppm) and lowest S (1007 ppm) concentrations; Cl^- may come from beach bioclasts in these mortars.

The chlorides probably originate from the sea[4]; therefore, some of this content could have entered the mortars even during use and after burial. On the other hand, the presence of S can be partially associated with the volcanic content in the mortars (Silva et al. 2007), together with the aerosols coming from the sea (Fossum et al. 2020) and anthropogenic contaminants. The conducted analyses show that the production technology of mortars, selection of raw materials, and environmental conditions affect the degree of hydraulicity and the chemical composition.

When the samples are classified according to their functions, lining mortars (MA-1, MA-10, MA-11, and MA-24) used in water related constructions would have been prepared with marly binder and ceramic aggregate and powder resulting in hydraulic to highly hydraulic properties. The only non-hydraulic sample MA-23 (vat lining) is the exception. Binders of rendering mortars (MA-2, MA-4, MA-6, MA-9, and MA-12) would probably have been prepared deliberately with only limestone to give the non-hydraulic property; however, the inner layers were prepared with marls (MA-2A, MA-8, MA-19, MA-22), ceramic (MA-17), and volcanic aggregates (MA-7 and MA-13) which increased the pozzolanic activity resulting in higher hydraulicity. Joint mortars (MA-3, MA-12, MA-20) have no hydraulic character, which implies the use of lean lime in manufacturing due to their use in non-water related structures. All bedding mortars for tiled floors (MA-5, MA-14, MA-15, MA-16, and MA-21) were prepared with volcanic aggregate and powder resulting in high hydraulicity. One possible scenario for the deliberate use of those aggregates is that probably builders could prepare the binders with limestone, the only available source at that time, and still needed hydraulicity because they wanted to keep the possible rising damp problem due to high water table under control.

Archaeological significance

In the later first century BCE, the classical historian Diodorus Siculus made remarks on the skilful architectural rendering of residences in Roman Malta (Diodorus Siculus, V.12. 1-4. 2012). Such craftsmanship has also been supported archaeologically with the discovery of numerous fragments of fine architectural *stucco*, mouldings, and decorative painted wall plaster (Bonanno 2005). However, it is only now that a full scientific assessment of such mortars and their constituent parts has been attempted. This section takes stock of these new scientific data and discusses the findings based on the available archaeological data. The following discussion will focus on two main aspects: (1) the archaeological significance of the source and potential function of the five types of mortars identified and (2) the potential chronological implications of these mortar types that can be gleaned from the archaeological phases of the site.

[4] Marine spray can travel several kilometres inland.

The samples belonging to Types 1, 2, and 3 include mortars used for masonry construction, renders, vat, cistern linings, and plain and painted wall renders. As discussed above, the composition of the binder and aggregates for these types suggest a source within the Maltese archipelago or even in the vicinity of the site (see 'Discussion'). Limited sections of painted wall render were discovered intact during the early excavations at the Villa, surviving along the interior 'residential' walls of the phase 2 of the villa (Bonanno and Vella 2012). Small fragments still survive, some of which have been studied macroscopically (Deguara 2015), as well as included in this study (i.e., MA-22). The layering of plaster visible in a number of these samples also follows the typical and well-known Roman technique of wall painting or *fresco*, where slaked lime mortars were applied to a surface, the coarser layers first, followed by successively finer layers, before bold pigments were applied to the smooth outer surface whilst the plaster was still wet. The current analyses confirmed that gradation from coarse and thick to fine and more elaborate layers on samples which exhibited at least two or more layers and which also confirmed previous work by Deguara (2015).

The three samples attributed to Type 4 all contain high concentrations of ceramic aggregate, typical of hard-wearing *cocciopesto* mortars of the Roman period. Although none of the samples could be directly linked to a physical building element at the site (they were all residual fragments associated with construction phase 2 or later), the composition and archaeological context support their function as fragments of flooring bedding which is further supported by the presence of similarly composed mortars from other Maltese sites of the same period, namely a series of *cocciopesto* floors dating to the second/first century BCE at the Late Punic/Roman sanctuary at Tas−Silġ, located a short distance from the Żejtun site (Bonzano 2017) and a similar floor adorning the courtyard of the olive press Villa complex at San Pawl Milqi dateable to the Imperial period (Bruno 2009). The presence of abundant ceramic aggregates as found in this present study also supports a local sourcing and manufacture of these mortars, presumably from recycled local ceramic pottery (Anastasi 2019), a conclusion also supported by the identification of the remains of globigerina in the ceramic fragments inside Type 4 mortars. The use of ceramic aggregate is well-known and is documented in Phoenician industrial complexes as early as the sixth century BCE in Lebanon (Orsinger et al. 2020) and Punic domestic architecture in Carthage in the fourth century BCE (Docter 2019). Such material was also particularly widespread during the Roman period both for the manufacture of floors, as well as hard-wearing, water-resistant linings for an array of vats and cisterns (Adam 1994). From an archaeological perspective, the mortars identified as Type 5 are of particular interest. Their volcanic aggregates are not available locally and could therefore have only been obtained by importing them into the islands. The use of volcanic sand-sized particles as temper in local clay amphorae and to line oil-collecting vats is well-documented in the Maltese Islands (Bruno and Capelli 2000; Bruno 2009). At the Żejtun Villa, however, the majority of the volcanic-rich mortar samples analysed were directly associated with bedding mortars used for floors laid with ceramic lozenge-shaped tiles sometime after the late second/first century BCE. Half of the Type 5 samples came from renders and a fragment of shuttering[5] (i.e., MA-7); thus, volcanic aggregate was not restricted to bedding mortars at the site, but neither was it used for other finishes, such as vat linings (i.e., MA-23 to Type 2), as would have been expected.

Of significance, however, is the composition of the binders across all the samples, including Type 5 mortars. They appear to be similar and likely sourced from the same local limestone material, although it occasionally, but not always, contained marly material. This further supports the hypothesis that the binder materials were indeed sourced, and the mortars, mixed locally, at times being supplemented with imported pozzolanic aggregate (or ceramic fragments) when required, or when these materials were available (Bruno 2009). Importing volcanic sand, whether directly or as a by-product of maritime trade (i.e., off-loaded ballast), has been documented historically (Burström, 2017) and explains its use as temper for local pottery types (Bruno 2009).

Based on the current archaeological evidence, the mortar samples, both those collected in situ and from later spoliation/levelling deposits, can be attributed to two possible major construction activities. One related to a pre-villa structure (phase 1) dated by pottery to the fourth to second centuries BCE, which was subsequently partly destroyed and expanded into the villa structure built shortly after the second/first century BCE (phase 2; Fig. 2, Tables 1 and 2). Demolition debris, including fragments of painted and plain wall plaster (MA-8, MA-9, MA-19), and mortars adhering to clearly re-utilised elements (MA-1, MA-20) belonged to structural elements that had already been demolished by the time the phase 2 Roman Villa was constructed, all of which included mortars of Types 1 to 3. All the mortars associated with Types 4 and 5 (with ceramic and volcanic aggregate respectively), together with a broad variety of Types 1 to 3 mortars, were all mixed and applied during or after the construction of the villa (phase 2). This suggests that the locally sourced limestone-based lime for mortars (Types 1–3) was used at the site as early as the Punic period, whilst mortars composed of ceramic and volcanic aggregate were applied to the Roman Villa, both during its initial construction, as well as for later extensions and maintenance works that are evident by the archaeological stratigraphy. Of particular interest, here is the clear introduction of an imported, volcanic aggregate used as bedding mortar to lay all the tiled floors at the site. The date

[5] Which still retained clear impressions left by the organic reeds used to support the mortar.

associated with the introduction of this type of aggregate use is also supported by the use of volcanic sand-sized particles in locally produced pottery, which became increasingly common in the Maltese Islands from the third to first centuries BCE onwards (Bruno 2009).

Conclusions

These first analyses of mortar samples from a Maltese archaeological site have identified five distinct mortar types used in the construction and decoration of an ancient Roman building. The analyses demonstrated a broad variety of mortar types that were mostly sourced and manufactured locally and were used for a diverse range of construction activities. A local source for the binders in all mortar types, as well as the aggregates used in four of the five types (Types 1–4), is highlighted. To prepare a hydraulic mortar, local pure limestone formations were often quarried, as Vitruvius noted, and the prepared air lime binder was mixed with reactive aggregate (rubefacted marl, bioclasts, ceramic, and volcanic rock fragments) and reactive additives (ash, ceramic powder). It has been detected that, occasionally, marl-bearing veins in limestone quarries or marl facies abundant in the local geology were also used to prepare hydraulic lime binders probably due to the lack of sufficient pure limestone deposits.

Aggregate/binder ratios vary among all mortar types. Type 2 mortars, most of which are renders, have high amount of aggregate (both limestone and bioclast fragments) and are used in the structures with no water contact. Ceramic and volcanic aggregates were used in similar amounts and less than some samples with limestone and bioclasts of Type 1–3.

The abundant volcanic aggregate in Type 5 mortars used mainly as a bedding mortar for ceramic tiled floors is a non-local resource; parallel archaeological evidence in pottery and mortars from other local Roman sites suggests that pozzolanic aggregate was imported to the islands from neighbouring volcanic regions.

This study has established a baseline by which archaeologists are able to characterise mortar composition, as well as its potential use in other archaeological sites, particularly relevant when only fragments of mortars and plasters survive devoid of their original context, as is often the case locally. There is strong potential for further analyses on mortars (and plasters), where samples collected in situ from recently excavated archaeological sites can be gathered and compared with this mortar typology.

Acknowledgements The authors are indebted to the Petrophysical Laboratory of IGEO (CSIC, UCM), the group of Petrology applied to the Heritage Conservation (921349). The authors wish to acknowledge professional support of the Interdisciplinary Thematic Platform from CSIC Open Heritage: Research and Society (PTI-PAIS).

Author contribution JC, MA, and NCV performed the sampling and wrote the historical context of the archaeological site. RF reported on the geological context and geochemical results. MJVM wrote the petrography, and DE wrote the hydraulicity analysis. All authors contributed to writing the discussion and conclusions and revised the final manuscript.

Funding Open Access funding provided thanks to the CRUE-CSIC agreement with Springer Nature. This research was funded by the project CLIMORTEC (BIA2014-53911-R) of Ministry of Economy and Competitiveness of Spain and the project TOP Heritage (P2018/NMT-4372) of the Community of Madrid.

Data availability Not applicable.

Code availability Not applicable.

Declarations

Competing interests The authors declare no competing interests.

Ethics approval Not applicable.

Consent to participate We give our consent.

Consent for publication We give our consent.

Conflict of interest The authors declare no competing interests.

Open Access This article is licensed under a Creative Commons Attribution 4.0 International License, which permits use, sharing, adaptation, distribution and reproduction in any medium or format, as long as you give appropriate credit to the original author(s) and the source, provide a link to the Creative Commons licence, and indicate if changes were made. The images or other third party material in this article are included in the article's Creative Commons licence, unless indicated otherwise in a credit line to the material. If material is not included in the article's Creative Commons licence and your intended use is not permitted by statutory regulation or exceeds the permitted use, you will need to obtain permission directly from the copyright holder. To view a copy of this licence, visit http://creativecommons.org/licenses/by/4.0/.

References

Adam JP (1994) Roman building: materials and techniques. Routledge, London, p 736

Anastasi M (2012) The Pottery from the 1972 excavations at the Zejtun villa. In: R. Abela, ed, The Zejtun Roman Villa: Research, Conservation, Management. Malta: Wirt iz-Zejtun, pp. 26–41

Anastasi M (2019) Pottery from Roman Malta. Archaeopress, Oxford

Anastasi M, Vella NC (2018) Olive oil production technology in Roman Malta, In: The lure of the antique: essays on Malta and Mediterranean archaeology in honour of Anthony Bonanno (Ancient Near Eastern Studies Supplement 54), edited by N.C. Vella, A.J. Frendo and H.C.R. Vella: 275–300. Leuven: Peeters

Anastasi M, Betts JC, Vella NC (2022). From windlass to screw: oil pressing technology in the Maltese islands in antiquity, In: Essays in honour of Horatio Caesar Roger Vella. Malta: Midsea Books, pp 39–61

Bakolas A, Biscontin G, Contardi V, Franceschi E, Moropoulou A, Palazz D, Zendri E (1995) Thermoanalytical research on traditional mortars in Venice. Thermochim Acta 269–270:817–828. https://doi.org/10.1016/0040-6031(95)02574-X

Baldassini, N, Di Stefano, A (2017) Stratigraphic features of the Maltese Archipelago: a synthesis. Nat Hazards 86: S203-S231. https://doi.org/10.1007/s11069-016-2334-9

Bianucci G, Gatt M, Catanzariti R, Sorbi S, Bonavia CG, Curmi R, Varola A (2011) Systematics, biostratigraphy and evolutionary patterns of the Oligo – Miocene marine mammals from the Maltese Islands. Geobes 44 (6): 549–585.https://doi.org/10.1016/j.geobios.2011.02.009

Biscontin G, Birelli MP, Zendri E (2002) Characterization of binders employed in the manufacture of Venetian historical mortars. J Cull Herit 3:31–37. https://doi.org/10.1016/S1296-2074(02)01156-1

Bonanno A (2005) Malta: Phoenician. Midsea Books Ltd, Malta, Punic and Roman, p 359

Bonanno A, Vella NC (2012) Past and present excavations of a multi-period site, in The Żejtun Villa: Research, Conservation, Management, edited by R. Abela: 8–25. Malta: Wirt iż-Żejtun.

Bonanno A (2018) Roman villas in the Maltese archipelago, in The Roman Villa in the Mediterranean Basin: Late Republic to Late Antiquity, edited by A. Marzano and G.P.R. Métraux: 255–265. Cambridge: Cambridge University Press.

Bonzano F (2017) Fanum Iunonis Melitense: L'area centrale del santuario di Tas-Silġ a Malta in età tardo-repubblicana. Bari: Edipuglia. 240 pp

Bruno B (2009). Roman and Byzantine Malta: trade and economy. Trans. by G. Cutajar in collaboration with P.J. Hudson. Malta: Midsea

Bruno B, Capelli C (2000) Nuovi tipi di anfore da trasporto a Malta, in C. d'Amico and C. Tampellini (eds) 6a Giornata Le scienze della terra e l'archeometria. Este, Museo Nazionale Atestino 26 e 27 febbraio 1999. Este: Grafica Atestina, pp. 59–65

Burström M (2017) Ballast: laden with history. Nordic Academic Press, Lund, p 120

Cangemi M, Di Leonardo R, Bellanca A, Cundy A, Neri R, Angelone M (2010) Geochemistry and mineralogy of sediments and authigenic carbonates from the Malta Plateau, Strait of Sicily (Central Mediterranean): relationships with mud/fluid release from a mud volcano system. Chem Geol 276(3–4):294–308. https://doi.org/10.1016/j.chemgeo.2010.06.014

Cardoso I, Macedo MF, Vermeulen F, Corsi C, Santos SA, Rosado L, Candeias A, Mirao J (2014) A multidisciplinary approach to the study of archaeological mortars from the town of Ammaia in the roman province of Lusitania (Portugal). Archeometry 56:1–24. https://doi.org/10.1111/arcm.12020

Chatzimpaloglou P, Schembri PJ, French C, Ruffell A, Stoddart S (2020) The geology, soils and present-day environment of Gozo and Malta, in C. French, C.O. Hunt, R. Grima, R. McLaughlin, S. Stoddart and C. Malone (eds), Temple landscapes: fragility, change and resilience of Holocene environments in the Maltese Islands (Fragsus, vol. 1). McDonald Institute for Archaeological Research, pp. 19–33

Columbu S, Garau AM (2017) Mineralogical, petrographic and chemical analysis of geomaterials used in the mortars of Roman Nora theater (south Sardinia, Italy). Italian Journal of Geosciences 136:238–262. https://doi.org/10.3301/IJG.2017.05

Columbu S, Sitzia F, Ennas G (2017) The ancient pozzolanic mortars and concretes of Heliocaminus baths in Hadrian's Villa (Tivoli, Italy). Archaeol Anthropol Sci 9:523–553. https://doi.org/10.1007/s12520-016-0385-1

Columbu S, Lisci C, Sitzia F, Lorenzetti G, Lezzerini M, Pagnotta S, Raneri S, Legnaioli S, Palleschi V, Gallello G, Adembri B (2018) Mineralogical, petrographic and physical-mechanical study of Roman construction materials from the Maritime Theatre of Hadrian's Villa (Rome, Italy). Measurement 127, 264–276. https://doi.org/10.1016/j.measurement.2018.05.103

Columbu S, Garau AM, Lugliè C (2019) Geochemical characterisation of pozzolanic obsidian glasses used in the ancient mortars of Nora Roman theatre (Sardinia, Italy): provenance of raw materials and historical–archaeological implications. Archaeol Anthropol Sci 11:2121–2150. https://doi.org/10.1007/s12520-018-0658-y

Craig H (1957) Isotopic standards for carbon and oxygen and correction factors for mass-spectrometric analysis of carbon dioxide. Geochemical and Cosmochemical Acta 12:133–149. https://doi.org/10.1016/0016-7037(57)90024-8

Deguara R (2015) Characterising and classifying archaeological plasters and mortars from Malta. MA dissertation. University of Malta.

Degryse P, Elsen J, Waelkens M (2002) Study of ancient mortars from Sagalassos (Turkey) in view of their conservation. Cement and Concrete Research 32:1457–1463. https://doi.org/10.1016/S0008-8846(02)00807-4

DeLaine J (2021) Production, transport and on-site organization of Roman mortars and plasters. Archaeol Anthropol Sci 13(11):195. https://doi.org/10.1007/s12520-021-01401-5

Dickson JAD (1966) Carbonate identification and genesis as revealed by staining. J Sediment Petrol 36:491–505

Diodoru Siculus (2012) (V.12 1-2) Biblioteca histórica. Madrid: Ed. Gredos, pp 550

Docter R (2019) Residential Architecture. In: López-Ruiz C, Doak BR (eds) The Oxford Handbook of the Phoenician and Punic Mediterranean. Oxford University Press, Oxford, pp 435–452

Dotsika E, Kyropoulou D, Christaras V, Diamantopoulos G (2018) ^{13}C and ^{18}O stable isotope analysis applied to detect technological variations and weathering processes of ancient lime and hydraulic mortars. Geociencies 8:339. https://doi.org/10.3390/geosciences8090339

Dotsika E, Psomiadis D, Poutoukis D, Raco B, Gamaletsos P (2009) Isotopic analysis for degradation diagnosis of calcite matrix in mortar. Anal Bioanal Chem. 395:2227–2234. https://doi.org/10.1007/s00216-009-3135-8

Drdácký M, Fratini F, Frankeová D, Slížková Z (2013) The roman mortars used in the construction of the Ponte di Augusto (Narni, Italy) - a comprehensive assessment. Constr Build Mater 38:1117–1128. https://doi.org/10.1016/j.conbuildmat.2012.09.044

Dunham RJ (1962) Classification of carbonate rocks according to depositional texture. In: Ham, W. E. (ed.), Classification of carbonate rocks: American Association of Petroleum Geologists Memoir, p. 108–121.

Elsen J (2006) Microscopy of historic mortars — a review. Cem Concr Res 36(8):1416–1424. https://doi.org/10.1016/j.cemconres.2005.12.006

Ergenç D, Fort R (2019) Multi-technical characterization of Roman mortars from Complutum. Spain Measurement 147:106876. https://doi.org/10.1016/j.measurement.2019.106876

Ergenç D, Fort R (2018) Accelerating carbonation in lime-based mortar in high CO2 environments. Constr Build Mater 188:314–325. https://doi.org/10.1016/j.conbuildmat.2018.08.125

Ergenç D, Fort R, Varas-Muriel MJ, Alvarez de Buergo M (2021) Mortars and plasters-How to characterize aerial mortars and plasters. Archaeol Anthropol Sci 13(11):197. https://doi.org/10.1007/s12520-021-01398-x

Fichera GV, Belfiore CM, La Russa MF, Ruffolo SA, Barca D, Frontoni R, Galli G, Pezzino A (2015) Limestone provenance in Roman lime-volcanic ash mortars from the Villa Dei Quintili. Rome Geoarcheology 30(2):79–99. https://doi.org/10.1002/gea.21504

Foresi LM, Baldassini N, Sagnotti L, Lirer F, Di Stefano A, Caricchi C, Verducci M, Salvatorini G, Mazzei R (2014) Integrated stratigraphy of the St. Thomas section (Malta Island): a reference section for the lower Burdigalian of the Mediterranean Region. Mar Micropaleontol 111:66–89. https://doi.org/10.1016/j.Marmicro.2014.06.004

Fort R, Ergenç D, Aly N, Alvarez de Buergo M, Hemeda S (2021) Implications of new mineral phases in the isotopic composition of Roman lime mortars at the Kom el-Dikka archaeological site in Egypt. Construction and building materials 268:121085. https://doi.org/10.1016/j.conbuildmat.2020.121085

Fossum KN, Ovadnevaite J, Ceburnis D, Preissler J, Snider JR, Huang RJ, Zuend, A, O'Dowd C (2020). Sea-ray regulates sulfate cloud

droplet activation over oceans. NPJ Climate and Atmospheric Science, 14. https://doi.org/10.1038/s41612-020-0116-2
Genestar C, Pons C, Más A (2006) Analytical characterization of ancient mortars from the archaeological Roman city of Pollentia (Balearic Islands, Spain). Anal Chim Acta 557:373–379. https://doi.org/10.1016/j.aca.2005.10.058
Gruszczynski M, Marshall JD, Goldring R, Coleman ML, Malkowski L, Gazdzicka E, Semil J, Gatt P (2008) Hiatal surfaces from the Miocene Globigerina Limestone Formation of Malta: biostratigraphy, sedimentology, trace fossils and early diagenesis. Palaeogeogr Palaeoclimatol Palaeoecol 270(2–3):239–251. https://doi.org/10.1016/j.palaeo.2008.01.035
Kosednar-Legenstein B, Dietzel M, Leis A, Stingl K (2008) Stable carbon and oxygen isotope investigation in historical lime mortar and plaster – results from field and experimental study. Appl Geochem 23:2425–2437. https://doi.org/10.1016/j.apgeochem.2008.05.003
Lancaster L (2021) Mortars and plasters-how mortars were made. The literary sources. Archaeological and Anthropological Sciences 13 (11):192.https://doi.org/10.1007/s12520-021-01395-0
Lawrence R (2006) A Study of carbonation in nonhydraulic lime mortars, PhD Dissertation, Bath: University of Bath
Miriello D, Antonelli F, Apollaro C, Bloise A, Bruno N, Catalano M, Columbu S, Crisci GM, De Luca R, Lezzerini M, Mancuso S, La Marca A (2015) A petro-chemical study of ancient mortars from the archaeological site of Kyme (Turkey). Period Mineral 84:497–517. https://doi.org/10.2451/2015PM0028
Morandeau A, Thiéry M, Dangla P (2014) Investigation of the carbonation mechanism of CH and C-S-H- in terms of kinetic, microstructure changes and moisture properties. Cem Concr Res 56:153–170. https://doi.org/10.1016/j.cemconres.2013.11.015
Morgan MH (1960) The ten books on architecture. Courier Dover Publications. 331 pp
Moropoulou A, Bakolas A, Bisbikou K (1995) Characterization of ancient, byzantine and later historic mortars by thermal and X-ray diffraction techniques. Thermochim Acta 269:779–795. https://doi.org/10.1016/0040-6031(95)02571-5
Moropoulou A, Bakolas AB, K. (2000) Investigation of the technology of historic mortars. J Cult Herit 1(1):45–58. https://doi.org/10.1016/S1296-2074(99)00118-1
Moropoulou A, Bakolas A, Anagnostopoulou S (2005) Composite materials in ancient structures. Cement Concr Compos 27:295–300. https://doi.org/10.1016/j.dibe.2022.100081
Noel PJ, Brian J (2016) Origin of carbonate sedimentary rocks. Wiley. 446p
Rodríguez-Navarro C (2004) Binders in historical buildings: Traditional lime in conservation. Seminario SEM 09:91–112
Pedley HM, Bennett SM (1985) Phosphorites, hardgrounds and syndepositional subsidence: a paleoenvironmental model from Miocene of the Maltese Islands. Sedimentary Geolology 45:1–34. https://doi.org/10.1016/0037-0738(85)90022-3
Pedley HM (1976) A palaeoecological study of the Upper Coralline Limestone, Terebratula-Aphelesia bed (Miocene, Malta) based on bryozoan growth-form studies and brachiopod distributions. Palaeogeogr Palaeoclimatol Palaeoecol 20:209–234. https://doi.org/10.1016/0031-0182(76)90003-1
Prendergast AL, Azzopardi M, O'Connell TC, Hunt C, Barker G, Stevens RE (2013) Oxygen isotopes from *Phorcus (Osilinus) turbinatus* shells as a proxy for sea surface temperature in the central Mediterranean: a case study from Malta. Chem Geol 345(8):77–86. https://doi.org/10.1016/j.chemgeo.2013.02.026
Rassineux F, Claude-Petit J, Meunier A (1989) Ancient analogues of modern cement: calcium hydrosilicates in mortars and concretes from Gallo-Roman thermal baths of western France. J Am Ceram Soc 72(6):1026–1032. https://doi.org/10.1111/j.1151-2916.1989.tb06263.x
Riccardi MP, Lezzerini M, Carò F, Franzini M, Messiga B (2007) Microtextural and microchemical studies of hydraulic ancient mortars: two analytical approaches to understand pre-industrial tech-nology processes. J Cult Herit 8:350–360. https://doi.org/10.1016/j.culher.2007.04.005
Rose EPF, Pratt SK, Bennett SM (1992) Evidence for sea-level changes in the Globigerina limestone formation (Miocene) of the Maltese Islands. Paleontol Evol 24–25:265–276
Scerri, S. (2019) Sedimentary Evolution and Resultant Geological Landscapes. In: Gauci, R., Schembri, J. (eds) Landscapes and landforms of the Maltese Islands. World Geomorphological Landscapes. Springer, Cham. https://doi.org/10.1007/978-3-030-15456-1_4
Seymour LM, Keenan-Jones D, Zanzi GL, Weaver JC, Masic A (2022) Reactive ceramic aggregates in mortars from ancient water infrastructure serving Rome and Pompeii. Cell Reports Physical Science 3(9):101024. https://doi.org/10.1016/j.xcrp.2022.101024
Silva B, Rivas T, García-Rodeja E, Prieto B (2007) Distribution of ions of marine origin in Galicia (NW Spain) as a function of distance from the sea. Atmos Environ 41(21):4396–4407. https://doi.org/10.1016/j.atmosenv.2007.01.045
Toffolo MB, Regev L, Mintz E, Kaplan-Ashiri I, Dubernet S, Yan X, Regev J, Boaretto E (2020) Structural characterization and thermal decomposition of lime binders allow accurate Radiocarbon age determinations of aerial lime plaster. Radiocarbon 62(3):633–655. https://doi.org/10.1017/RDC.2020.39
Uğurlu Sağın, E. Duran, H.E. Böke, H (2021) Lime mortar technology in ancient eastern Roman provinces, Journal of Archaeological Science: Reports, 39, 103132, https://doi.org/10.1016/j.jasrep.2021.103132
Van Strydonck M, Dupas M, Dauchotdehon M, Pachiaudi C, Marechal J (1986) The influence of contaminating (fossil) carbonate and the variations of delta-c-13 in mortar dating. Radiocarbon 28:702–710. https://doi.org/10.1017/S003382220000792X
Vella NC, Bonanno A, Anastasi M, Bechtold B, Farrugia R, Fenech K, Mizzi D, Verdonck L, Zammit AR (2018) A view from the countryside: the nature of the Late Punic and Early Roman activity at the Żejtun Villa site, Malta. Rivista di Studi Fenici 45:109-143
Vitti P (2021) Mortars and masonry-structural lime and gypsum mortars in Antiquity and Middle Ages. Archaeol Anthropol Sci 13(10):164. https://doi.org/10.1007/s12520-021-01408-y
Yaseen IAB, Al-Amoush H, Al-Farajat M, Mayyas A (2013) Petrography and mineralogy of Roman mortars from buildings of the ancient city of Jerash. Jordan Constr Build Mater 38:465–471. https://doi.org/10.1016/j,conbuildmat.2012.08.022

Publisher's note Springer Nature remains neutral with regard to jurisdictional claims in published maps and institutional affiliations.